Journal of Biochemical and Molecular Toxicology

WILEY

RESEARCH ARTICLE

A Small Indole Derivative Isolated From Caper (*Capparis ovata*) as an Inducer of P53-Mediated Apoptosis in Prostate Cancer: Comprehensive In Vitro and In Silico Studies

Özden Özgün Acar[1] | Işıl Gazioğlu[2] | Hatice Oruç[3] | Elif Kale[4] | Halil Şenol[5] | Gülaçtı Topçu[6] | Alaattin Şen[4,7]

[1]Health Services Vocational School of Higher Education, Pamukkale University, Denizli, Türkiye | [2]Department of Analytical Chemistry, Faculty of Pharmacy, Bezmialem Vakif University, Istanbul, Türkiye | [3]Department of Biology, Faculty of Sciences, Pamukkale University, Denizli, Türkiye | [4]Department of Biology, Faculty of Sciences, Kocaeli University, Kocaeli, Türkiye | [5]Department of Pharmaceutical Chemistry, Faculty of Pharmacy, Bezmialem Vakif University, Istanbul, Türkiye | [6]Department of Pharmacognosy & Phytochemistry, Faculty of Pharmacy, Bezmialem Vakif University, Istanbul, Türkiye | [7]Department of Molecular Biology & Genetics, Faculty of Natural & Life Sciences, Abdullah Gul University, Kayseri, Türkiye

Correspondence: Halil Şenol (hsenol@bezmialem.edu.tr) | Alaattin Şen (sena@agu.edu.tr)

Received: 22 July 2025 | **Revised:** 9 December 2025 | **Accepted:** 19 December 2025

Funding: Scientific and Technological Research Council of Turkey; Pamukkale Universit

Keywords: anti-cancer | Indole-2-hydroxy-3-carboxylic acid | molecular docking | molecular dynamics | P53

ABSTRACT

Natural products with stunning chemical diversity have been extensively researched for their anticancer potential for more than fifty years. This study aimed to determine the effect of indole derivative 1*H*-indole-2-hydroxy-3-carboxylic acid (IHCA), isolated as a novel alkaloid from *Capparis ovata*, on selected tumor suppressor, apoptotic, and cell cycle regulatory genes, which are known to be important in cancer pathophysiology, on Caco-2 and LNCaP cells in comparison with Taxol. The molecular mechanism of IHCA's anticancer activity is essentially undefined. Different concentrations of IHCA increased the expression levels of apoptosis-related genes, including BCL-2 and TNF-α. In addition, the tumor suppressor genes PTEN, P53, and RB were increased in LNCaP and Caco-2 cells. KRAS, an oncogenic gene, was significantly downregulated by IHCA in LNCaP cells. Western blot results showed that the protein expression levels of P53 and PTEN in LNCaP cells were increased when treated with IHCA, whereas CDK4 and TNF-α were decreased. Finally, IHCA and doxorubicin significantly increased P53-driven luciferase activity compared to the control. The results strongly suggest that the novel natural compound IHCA has an anticancer effect involving the regulation of the P53 gene and its networks in vitro. The molecular docking and MD simulation analyses reveal that IHCA exhibits superior binding potential to the MDM2 protein compared to Nutlin-3a. MD simulations further confirm that IHCA maintains a more stable and consistent interaction with MDM2, as indicated by lower RMSD values and reduced ligand fluctuation. These results highlight IHCA's potential as a more effective MDM2 inhibitor, suggesting its promise as a lead compound for anticancer drug development.

Clinical Trial Registration: Not applicable.

1 | Introduction

Cancer is the most common cause of death in the world. It is the second main reason for mortality after cardiovascular diseases, and the mortality caused by cancers is increasing throughout the world [1]. Cancer is anticipated to be the primary reason for death and the most significant barrier to increasing life expectancy globally in this century. For both men and women, colorectal cancer (10.2%) and prostate cancer

(7.1%) are the second and third most frequent cancers, respectively, and the third and seventh leading causes of death worldwide [2–4]. Thus, studies for better drugs that are effective in chemoprevention and treatment continue to improve efficiency and decrease cancer care costs. Recently, plants and their secondary metabolites, called the specific term "natural products," have attracted significant attention as cancer chemopreventive agents and cancer therapeutics [5]. Taxol, one of the most effective cancer-treating agents to date, was discovered as the active ingredient of *Taxus brevifolia*, which has a taxane diterpene skeleton with a nitrogen atom in the side chain. Additionally, numerous natural alkaloids with indole skeletons have shown anti-inflammatory and cytotoxic/anticancer activities, particularly bis-indole alkaloids, which have been used to treat cancers such as vinblastine and vincristine [6].

The discovery of anticancer drugs focuses on nitrogen-containing heterocycles, including indole-based compounds, because these compounds interact with DNA, enzymes, receptors, and redox systems through π–π stacking, hydrogen bonding, and metal coordination. The antiproliferative and pro-apoptotic effects of indole derivatives, including indole-3-carbinol, indole-3-carboxylic acid, indole-2-carboxylic acid, and 1*H*-indole-2,3-dione (isatin), have been proven in multiple cancer cell lines [7–11]. The development of 1*H*-indole-2,3-dione and indolin-2-one derivatives has established them as well-settled anticancer drug candidates. Research studies show that isatin-based hybrids possess the ability to block multiple cancer-promoting kinases, including VEGFR-2, EGFR, CDK2, and STAT3, as well as blocking tumor carbonic anhydrase enzymes and disrupting tubulin structures, activating mitochondrial apoptosis and caspase activation in breast, colon, liver, lung, and drug-resistant cancer cells [8]. The indole compound 1*H*-indole-2-hydroxy-3-carboxylic acid (IHCA) shows an interesting structure, but its potential has not been fully explored. IHCA has been discovered as a new alkaloid from Capparis ovata plants while studying its neurological effects, anti-inflammatory properties, and anticancer activity [10, 12–15]. The research findings about IHCA exist only in national thesis reports and meeting abstracts but have not received international publication for detailed mechanistic studies. The lack of understanding about IHCA's anticancer mechanism stands in contrast to other indole-based agents because its molecular action is essentially undefined.

One of the essential medicinal plants in Turkey is the *Capparis* species. Caper parts such as flower buds, root bark, and fruits are used in traditional medicine due to analgesic, wound-healing, tonic, and diuretic effects. Plant parts, especially flower buds, show antioxidant, cell regeneration, anticancer, and anti-inflammatory activities against multiple sclerosis [16–22]. A recent study evaluated the cytotoxicity of some flavonoids, including quercetin, kaempferol, and isorhamnetin derivatives, isolated from *C. spinosa var. aegytiaca* ethanolic extract against three human cancer cell lines, breast (MCF-7), liver (HEPG-2) and colon (HCT-116), and flavonoids exhibited significant effects [23]. Anatolian *C. spinosa* was studied for its secondary metabolites by the Calis group, and 1*H*-indole-3-acetonitrile glycosides and *(6S)*-hydroxy-3-oxo-α-ionol glucosides were obtained from its fruit extract [24, 25]. Additionally, two indole molecules, 1*H*-indole 3-carboxyaldehyde and 4-hydroxy-1*H*-indole 3-carboxyaldehyde, showing anti-inflammatory potential, were obtained from the fruits of *C. spinosa* [26]. A preliminary bioactivity assessment of ethanol and ethyl acetate extracts of *C. dognvanensis* leaves indicated that both extracts inhibited HeLa, A549, MCF7, RD, and HepG2 cancer cells [27].

P53-mediated apoptosis is a process in which the tumor suppressor protein P53 triggers programmed cell death (apoptosis) in response to cellular stress or DNA damage. P53 acts as a guardian of the genome by monitoring cell integrity. When it detects DNA damage or other stress signals, P53 becomes activated and can either halt cell division to allow for DNA repair or initiate apoptosis if the damage is irreparable.

The apoptotic function of P53 is primarily executed through the transcriptional activation of pro-apoptotic genes, such as BAX, PUMA, and NOXA. These genes lead to the permeabilization of the mitochondrial outer membrane, releasing cytochrome c into the cytoplasm, which then activates the caspase cascade, ultimately leading to cell death. By inducing apoptosis, P53 prevents the propagation of damaged cells, thus protecting the organism from potential cancer development [28, 29].

In this study, 1*H*-indole-2-hydroxy-3-carboxylic acid (IHCA) was isolated from a dichloromethane extract of *Capparis ovata* as a novel compound and is new to the literature in our previously published work [30] (Figure 1). Many natural and synthetic indole-containing compounds have been shown to affect numerous signaling pathways and are promising anticancer agents in either disease models or cancer cell lines [31–34]. These studies give indole and its derivatives a prominent place in developing anticancer agents. Thus, the present study was undertaken to gain insight into the anticancer activity and mechanism of IHCA isolated from *Capparis ovata*. For this investigation, the IHCA was tested on selected tumor suppressor genes and apoptotic and cell cycle regulator genes known to be important in cancer pathophysiology in LNCaP (human lymph node carcinoma of the prostate) and Caco-2 (Cancer coli-2, human colorectal adenocarcinoma) cells. Additionally, molecular docking and molecular dynamics (MD) simulations were performed to investigate the mechanistic aspects of IHCA's inhibition of MDM2. The *in silico* results indicated that IHCA exhibits a more promising inhibitory potential compared to the reference MDM2 inhibitor, Nutlin-3a.

2 | Results and Discussion

2.1 | Isolation and Characterization of 1*H*-indole-2-hydroxy-3-carboxylic Acid (IHCA)

1*H*-indole-2-hydroxy-3-carboxylic acid (IHCA) was previously isolated and structurally characterized from a typical caper extract (*Capparis ovata*) in our earlier studies. IHCA is an alkaloid, and in the present study, its anticancer activity was evaluated for the first time. We have previously reported that

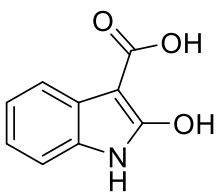

1*H*-indole-2-hydroxy-3-carboxylic acid (IHCA)

FIGURE 1 | Chemical structure of IHCA.

Capparis ovata is rich in phytochemicals such as terpenoids, steroids, flavonoids, and their glycosylated derivatives [17].

A compound with an indole ring was obtained from the dichloromethane (COWE-D) sub-extract of the primary water extract (COWE). The structure of this compound was found to be similar to the indole carboxylic acids previously isolated and characterized by our group from *Capparis spinosa* samples collected from Central Turkey. In the present study, the biological activity of IHCA was investigated for the first time [35]. The spectroscopic characteristics of 1*H*-indole-2-hydroxy-3-carboxylic acid obtained in this study are in full agreement with previously reported indole carboxylic acids, and these earlier works have now been properly cited. The ^{1}H-NMR data showed the typical four aromatic protons of the indole ring at δ 6.66–7.88, presenting the same splitting pattern and chemical shift range described in prior studies. Likewise, the ^{13}C-NMR spectrum exhibited methine carbons at δ 115–131 ppm and quaternary carbons at δ 162–174 ppm, consistent with the established substitution pattern of a hydroxyl group at C-2 and a carboxylic acid at C-3. The downfield carbonyl signal at δ 174 ppm and the characteristic deshielded C-2 resonance at δ 162.5 ppm further corroborate the structural features previously documented. These matching NMR profiles confirm that the isolated compound corresponds to the same indole derivative reported in earlier literature [17, 35].

2.2 | Effects of IHCA and Taxol on Cell Viability

To study the effect of IHCA on the growth of LNCaP and Caco-2 cells, a cell proliferation assay was carried out using crystal violet at different concentrations of IHCA along with Taxol for 24 h. IHCA inhibited the growth of both LNCaP and Caco-2 cells in a dose-dependent manner (Figure 2a). At 24 h, the proliferation of LNCaP and CaCo-2 cells was significantly inhibited at 200 μM and 217 μM IHCA, respectively. Although these concentrations were much higher than those obtained with the control drug Taxol (Figure 2b), they are compatible with the EC_{50} values reported for natural indole compounds [36]. The EC25 and EC50 values for IHCA were calculated to be 56 ± 1.53 μM and 200 ± 5.04 μM in Caco-2 cells, and 58 ± 3.51 μM and 217 ± 6.56 μM in LNCaP cells, respectively. The EC_{25} and EC_{50} values of Taxol were 2.3 ± 0.14 nM and 9.3 ± 0.56 nM in Caco-2 cells and 3 ± 0.18 nM and 15.2 ± 0.39 nM in LNCaP cells, respectively (Figure 2b). Thus, IHCA is not an inhibitor of cell proliferation as potent as Taxol, but the growth of both cancer cell lines was inhibited in a concentration-dependent manner.

The results show IHCA blocks cell growth, but its EC_{50} values between 200 and 217 μM make it less effective than conventional cancer drugs like paclitaxel (Taxol), which shows low-nanomolar activity in scientific studies. The unknown therapeutic potential of IHCA in humans remains unclear because of its high concentration levels. The high EC_{50} value of IHCA indicates that its current form will not achieve therapeutic levels when used as a standard systemic cancer treatment. The high EC_{50} value of IHCA makes the compound suitable for additional development work instead of rendering it useless for scientific studies. The compound shows minimal harm to normal cells at high concentrations, which makes it suitable for oral chemoprevention treatment when high tissue drug levels are acceptable, but systemic drug exposure remains low. The experimental data shows that IHCA needs to serve as an initial drug development platform instead of being treated as a finished pharmaceutical product.

2.3 | Effects of IHCA and Taxol on the Expression of Selected Genes at the mRNA Level

The effects of IHCA and Taxol on the expression of selected genes were determined in each cell line to reveal the molecular mechanisms underlying their antiproliferative actions (Table 1). Across both LNCaP and Caco-2 cells, IHCA shows a very consistent activation of classical tumor suppressor pathways, much more coordinated than Taxol. For both cell lines, the mRNA levels of only three genes were significantly altered with treatment at EC_{25} of IHCA, and these were primarily oncogenic and tumor suppressor genes, such as PTEN and RB. However, most of the studied genes were affected by IHCA treatment at EC_{50}. Significant tumor suppressor genes, such as PTEN (phosphatase and tensin homolog), P53 (TP53, tumor protein 53), and RB

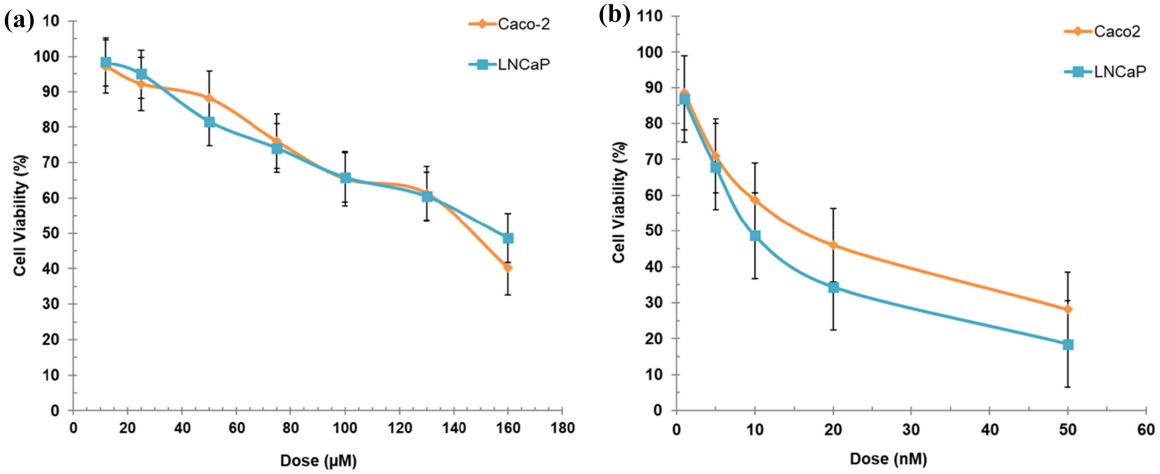

FIGURE 2 | Cytotoxicity of IHCA (a) on Caco-2 and LNCaP cells and Taxol (b) on Caco-2 and LNCaP cells. Cells were treated with increasing concentrations of IHCA and Taxol for 24 h, and cell viability was determined by crystal violet staining. The results are expressed as mean ± SE of three independent experiments performed in triplicate.

TABLE 1 | The expression levels of the selected genes at the mRNA level in LNCaP and Caco-2 cell lines treated with EC_{25} and EC_{50} doses of IHCA and Taxol.

Gene	LNCaP Cell line				Caco-2 cell line			
	IHCA		Taxol		IHCA		Taxol	
	EC_{25}	EC_{50}	EC_{25}	EC_{50}	EC_{25}	EC_{50}	EC_{25}	EC_{50}
Regulation of apoptosis								
BAX	1.27 ± 0.1	1.1 ± 0.06	−1.11 ± 0.07	−2.29 ± 0.2	1.01 ± 0.04	−1.18 ± 0.2	−2.39 ± 0.21	−2.69 ± 0.38
BCL2	−1.24 ± 0.3	−2.56 ± 0.07	−14.41 ± 0.63	−20.54 ± 0.56	1.02 ± 0.14	−2.07 ± 0.04	−6.96 ± 0.31	−9.74 ± 0.14
FAS	1.37 ± 0.06	1.02 ± 0.12	−6.15 ± 0.13	−6.25 ± 0.34	1.54 ± 0.05	−1.05 ± 0.44	−4.24 ± 0.38	−3.85 ± 0.38
TNF	−6.14 ± 0.28	−6.77 ± 0.4	−1.55 ± 0.07	−3.92 ± 0.25	−1.39 ± 0.02	−2.81 ± 0.36	−3.59 ± 0.08	−2.79 ± 0.52
Caspase and regulators								
APAF1	1.2 ± 0.21	1.44 ± 0.43	−2.53 ± 0.21	−2.87 ± 0.32	1.63 ± 0.16	4.07 ± 0.07	−3.93 ± 0.06	1.27 ± 0.28
CASP3	1.31 ± 0.24	1.27 ± 0.18	−8.85 ± 0.38	−6.5 ± 0.21	1.43 ± 0.07	2.73 ± 0.2	−4.53 ± 0.06	−3.01 ± 0.3
CASP8	1.49 ± 0.03	1.42 ± 0.02	−1.22 ± 0.67	1.01 ± 0.22	1.24 ± 0.05	1.04 ± 0.43	−2.27 ± 0.26	−2.59 ± 0.09
CASP9	1.72 ± 0.07	1.04 ± 0.33	1.18 ± 0.32	−5.11 ± 0.61	1.33 ± 0.13	2.61 ± 0.14	−14.72 ± 0.36	−10.66 ± 0.41
Oncogenic and tumor suppressor genes								
c-MYC	1.6 ± 0.2	1.13 ± 0.44	−2.14 ± 0.07	−12.39 ± 0.33	1.45 ± 0.03	−1.58 ± 0.15	2.14 ± 0.23	−1.07 ± 0.14
KRAS	−2.47 ± 0.20	−7.59 ± 0.17	−1.44 ± 0.02	−1.68 ± 0.31	1.12 ± 0.04	1.44 ± 0.18	−3.84 ± 0.03	−2.25 ± 0.021
PTEN	1.47 ± 0.31	8.93 ± 0.52	−1.96 ± 0.04	−2.33 ± 0.17	3.91 ± 0.17	5.22 ± 0.15	−1.46 ± 0.04	2.45 ± 0.17
P53	1.1 ± 0.29	4.03 ± 0.07	−3.04 ± 0.32	4.29 ± 0.52	1.77 ± 0.2	3.45 ± 0.12	1.22 ± 0.16	1.53 ± 0.12
RB	3.85 ± 0.38	2.5 ± 0.14	−1.19 ± 0.08	−5.75 ± 0.34	2.71 ± 0.04	2.44 ± 0.03	−2.42 ± 0.08	−3.34 ± 0.32
Regulation of cell cycle								
CDK4	−2.14 ± 0.06	−6.86 ± 0.27	−4.58 ± 0.23	−2.25 ± 0.09	−1.09 ± 0.07	−1.13 ± 0.16	−14.87 ± 0.28	−4.3 ± 0.02
CYCD2	1.54 ± 0.41	1.9 ± 0.26	−2.5 ± 0.16	−2.56 ± 0.03	−3.23 ± 0.04	−2.18 ± 0.13	−1.96 ± 0.18	−1.79 ± 0.25
Others								
ERK	3.64 ± 0.14	3.7 ± 0.018	7.43 ± 0.19	−5.58 ± 0.28	−1.01 ± 0.07	−1.18 ± 0.11	−2.17 ± 0.23	−1.96 ± 0.08
JNK	−2.26 ± 0.08	−2.18 ± 0.12	−1.74 ± 0.15	−4.41 ± 0.62	1.21 ± 0.15	1.43 ± 0.21	−2.4 ± 0.23	−2.9 ± 0.41

(pRB, retinoblastoma protein), were increased 8.9-fold, fourfold, and 2.5-fold, respectively, with IHCA in LNCaP cells. Similarly, the EC_{50} dose of IHCA increased the same genes but slightly to lower extents within the Caco-2 cell line. The coordinated activation mechanism explains IHCA through its evidence that treatment activates particular tumor-suppressing genes instead of causing random toxic effects.

In addition, genes associated with the regulation of apoptosis, such as BCL-2 (B-cell lymphoma 2) and TNF-α (tumor necrosis factor-alpha), were significantly decreased with IHCA in both cell lines, and the suppression levels were higher in LNCaP cells than in Caco-2 cells. For example, TNF-α mRNA levels were reduced by 6.1-fold in LNCaP cells and 2.8-fold in Caco-2 cells. Although Caspases 3, 8, and 9 (CASP3, CASP8, and CASP9) and APAF1 (apoptotic peptidase activating factor 1) mRNA levels were not altered statistically in LNCaP cells, the mRNA expression levels of APAF, CASP3, and CASP9 were increased 4.1-fold, 2.7-fold, and 2.6-fold, respectively, following EC_{50} IHCA treatment in Caco-2 cells. The two lines show IHCA triggers caspase activation while it decreases BCL2 protein levels but does not lead to significant BAX protein accumulation. The apoptosis process depends primarily on p53–PTEN–APAF1–caspase signaling and BCL2 suppression instead of BAX overexpression. The treatment process triggers both intrinsic and effector caspase pathways to cause cell death, but it also prevents the production of pro-inflammatory cytokine TNF. TNF protein functions as a dual agent, which causes apoptosis and necroptosis but leads to chronic inflammation and tumor growth through NF-κB activation. The treatment profile of IHCA distinguishes between cell death and TNF-induced inflammation through p53 activation and caspase activation for cancer cell death and TNF blockade and JNK level reduction in LNCaP cells. The treatment approach could prevent TNF from creating conditions that support tumor growth in the surrounding tissue.

The proto-oncogene KRAS (Kirsten rat sarcoma viral oncogene homolog), which promotes cell growth and proliferation, was significantly downregulated with IHCA treatment in LNCaP cells but not significantly altered in Caco-2 cells. Similarly, the CDK4 (cyclin-dependent kinase 4) gene associated with tumorigenesis was reduced significantly in LNCaP cells but not significantly altered in Caco-2 cells. While ERK (extracellular regulated kinase) mRNA levels were increased significantly, JNK mRNA levels decreased significantly, followed by EC_{50} values of IHCA treatment with LNCaP cells. No significant changes were observed with these genes in Caco-2 cells.

The single and double underlined figures indicate significantly decreased (blue) and increased (red) values, respectively, compared to control values ($p < 0.05$). Data are given as Mean ± SD.

Taxol, the brand name for paclitaxel, is a chemotherapeutic agent used to treat various cancers and was used as a positive control agent in this study. It inhibited the expression of almost all the genes examined except P53 and PTEN in LNCaP and Caco-2 cell lines, respectively. The mRNA levels of these two genes were increased 4.3-fold and 2.4-fold, respectively. On the other hand, mRNA levels of the rest of the genes studied were suppressed at a range of 1- to 21-fold. The gene-expression pattern demonstrates IHCA functions mainly as a tumor-suppressor pathway activator through the p53/PTEN/RB axis with different mechanisms than Taxol's microtubule disruption approach.

Since colorectal cancer (10.2%) and prostate cancer (7.1%) are the second and third most frequent cancers and leading causes of death worldwide (Bray et al., 2018), we studied the anticancer effect of IHCA using LNCaP (prostatic adenocarcinoma) and Caco-2 (colorectal adenocarcinoma) cell lines. Additionally, indole derivatives are an essential suppressor of the proliferation of colon and prostate cancer cell lines, as well as breast and endometrial cancer cells [37–39]. Although malignant growth is primarily characterized by limitless cell division and proliferation, its pathogenesis is incredibly intricate, and numerous components are involved. As the hallmarks of cancer comprise ten biological capabilities acquired during the multistep development of tumors [40]. Studies on the development of anticancer agents have examined their effects on these specific steps. Thus, we studied the effect of IHCA on three of these hallmarks, namely, proliferative signaling, cell death, and growth suppressors.

The P53 tumor suppressor is an excellent barrier to neoplastic transformation and tumor progression, with its ability to act as a highly sensitive collector of various inputs and maintain cellular homeostasis and genome stability [28]. It regulates hundreds of genes involved in multiple biological processes, including DNA damage repair, cell cycle, apoptosis, and aging, and coordinates various effector pathways and processes [29]. In this respect, it is an essential feature of anticancer agents to increase P53 transcriptional activity, and IHCA showed a significant increase in P53 expression in both cell lines. It is strongly feasible when the effects of the new natural IHCA, which is the first time in this study, are reported to the literature on the expression of the genes examined.

It has an anticancer action involving the regulation of the P53 tumor suppressor gene and its networks. An increase in P53 levels triggered by IHCA inhibits the growth of cancer cells and induces apoptosis by regulating the suppression of the pro-apoptotic BCL2 protein family and CYCD2 and CDK4 genes involved in the regulation of the cell cycle and apoptosis. Similar relationships between P53 and these genes were also reported [41–43]. In addition, the observed changes in PTEN gene expression levels with the application of IHCA support this mechanism since it is known that P53-mediated apoptosis is impaired in PTEN-null mouse embryonic fibroblasts, and the potential importance of PTEN transactivation for this procedure has been reported [44]. Therefore, IHCA involves PTEN activation-mediated apoptotic effects in both cell lines by increasing P53 expression levels. This effect appears to occur at a much higher level in the prostate cell line. In addition, IHCA is also an effective and selective anticancer agent because it induces the expression levels of both P53 and PTEN tumor suppressor genes.

The functional interactions between P53 and PTEN and their regulated pathways are essential for the therapeutic aspects of anticancer agents [44–46]. Moreover, the results observed at the mRNA level were also confirmed at the protein level, particularly for the LNCaP cell line. As a result, *1H*-indole-2-hydroxy-3-carboxylic acid has been observed to induce apoptosis and block the cell cycle via P53 regulation, particularly in prostate cancer cells. In addition, increases in the expression levels of RB, another critical tumor suppressor protein, further support the proposed mechanism and suggest that the cell cycle is very likely to be arrested in the G1 phase [47]. Although the

observed decreases in TNF-α expression levels with IHCA treatment seem to contradict the apoptotic effects of this compound, it overlaps with the recommended general mechanism and anticancer effect of the compound because the TNF-α paradox is a well-known phenomenon in cancer progression and cancer immunotherapy [48, 49].

As a pro-inflammatory cytokine, TNF-α plays a role in inflammation-related carcinogenesis. On the other hand, TNF-α could be an efficient cancer killer by inducing apoptosis. In this study, the induction of TNF-α and the associated suppression of JNK expression with IHCA treatment were considered to suppress inflammation-mediated carcinogenesis because the anti-inflammatory effects of indole-derived compounds via TNF-α suppression are known [50]. The induction of apoptosis by IHCA mediated via tumor suppressor genes, particularly through P53, was further confirmed by detecting parallel changes in the expression of executioner caspases such as Caspases 3 and 9 and the regulatory genes APAF1 and CYT-C. Caspase 9 and Caspase 3 have been shown to play an essential role in mitochondria-mediated apoptosis in human cells [51, 52]. While the effect of IHCA was not statistically significant in prostate cancer cells, significant increases were observed in Caco-2 cells. This suggests that IHCA adapts to different mechanisms in different cell lines. This difference is thought to result from differences in the metabolic pathways, genetic mutations, and metastatic potentials of the two cell lines [53, 54]. Nevertheless, IHCA probably has a selective action mechanism because it only affected a particular group of the genes, while the Taxol used as a positive control drug suppressed all the genes studied. The literature also reported that Taxol is not selective and has serious side effects [55–57]. At this point, it is possible to imply that IHCA is a more promising anticancer agent with a low potential for side effects.

The tumor-suppressor response of IHCA showed similar patterns in prostate (LNCaP) and colorectal (Caco-2) cancer cells through P53 and PTEN and RB up-regulation, but the apoptosis execution pathways showed different patterns based on their genetic profiles. The LNCaP cells, which have PTEN mutations and show constant AKT activation [58], showed significant PTEN restoration with elevated P53 and RB levels, but they only slightly increased APAF1 and CASP9 and CASP3 expression. The weak intrinsic caspase response in LNCaP cells matches their APAF1-ALT expression, which creates an impaired apoptosome function that slows down DNA damage-induced apoptosis and reduces its dependence on caspase-9 [59]. The tumor-suppressor reprogramming effects of IHCA in LNCaP cells lead cells to evade PI3K/AKT survival signals and apoptosome defects, which results in a weakened intrinsic apoptotic response. The Caco-2 colorectal cells show wild-type KRAS, BRAF, PIK3CA and PTEN genes but have a nonsense TP53 E204X mutation [60], and IHCA treatment led to strong APAF1, CASP9 and CASP3 expression along with BCL2 down-regulation, which indicates strong mitochondria-dependent apoptosis through caspase-9 activation. The research shows that Caco-2 cells and similar colorectal cancer models respond strongly to 5-fluorouracil and extracellular adenosine through caspase-9/3 activation and mitochondrial damage [61, 62]. The indole scaffold (IHCA) produces different effects on cancer cells because it triggers tumor suppressor functions in PTEN-null APAF1-ALT-expressing LNCaP cells through a caspase-independent mechanism, while it triggers a powerful p53-independent intrinsic apoptotic pathway in p53-deficient Caco-2 cells.

The compounds 3,3′-diindolylmethane (DIM) and indole-3-carboxylic acid (I3CA) share indole-3-carbinol (I3C) structural components, but they show different characteristics. The ATM–p53 pathway becomes active when I3C treatment occurs, which leads to p53 protein stabilization and activation of p21 and G_1 cell cycle arrest and modification of PI3K/AKT and NF-κB signaling pathways in various cancer cell lines, including mammary and melanoma cells [63–66]. The compound DIM causes cell growth arrest and programmed cell death in various cancer types through its ability to modify Bax/Bcl-2 ratios and activate caspases and MAPK/p38 and p21WAF1/CIP1 pathways [66–68]. The compound I3CA shows both chemosensitizing properties and direct anticancer effects through its ability to induce doxorubicin-mediated senescence and growth arrest in LS180 colorectal cells both in laboratory tests and animal models, and it exhibits native anticancer activity against lung cancer cells derived from Halymenia durvillei red algae [11, 69]. The indole-carboxylate structure of IHCA triggers p53 up-regulation and PTEN modulation and caspase activation but our research demonstrates separate P53–PTEN–RB activation patterns in LNCaP and Caco-2 cells and reduced TNF levels with no change in intrinsic apoptosis. The research community studies I3C and DIM as dietary compounds that affect hormone-dependent signaling pathways at low doses for cancer prevention, but IHCA shows better potential for mechanism-based development. The natural indole compounds activate p53/AKT/Bcl-2 networks through network reorganization, but IHCA functions through an independent transcriptional pathway that activates multiple tumor suppressor genes and blocks TNF signaling [63–68]. The anti-TNF effects of IHCA make it suitable for treating tumors that depend on inflammatory TNF signaling for their growth.

2.4 | Effects of IHCA and Taxol on the Expression of Selected Genes at the Protein Level

We performed Western blotting for the genes significantly altered at the mRNA level in LNCaP and Caco-2 cells by treatment with IHCA at the EC_{50} dose (Figure 3). As shown in Figure 3, the protein expression level of APAF1 was increased by 24%, and the PTEN level was decreased by 30% in the Caco-2 cell line. The administration of IHCA to LNCaP cells at the EC_{50} dose resulted in 49.7% and 56.3% reductions in the protein levels of CDK4 and TNF-α, respectively. P53 and PTEN protein levels were increased by 33.2% and 22.8%, respectively.

The Western blot results support the mRNA expression findings and provide additional details about the protein expression patterns. The protein expression patterns in LNCaP cells follow the same direction as the transcript data show. IHCA at EC_{50} reduces CDK4 mRNA levels by 6.9-fold and TNF mRNA levels by 6.8-fold, which results in 50% and 56% decreases in CDK4 and TNF-α protein levels, respectively. The protein levels of P53 and PTEN increase by 33.2% and a 22.8%, respectively, which matches the strong transcriptional activation of these genes by IHCA. The protein levels of P53 and PTEN show a 33.2% increase and 22.8% increase, respectively, which confirms that IHCA activates tumor suppressor pathways in LNCaP cells through changes at both mRNA and protein levels. The APAF1 mRNA levels in Caco-2 cells increase by fourfold after IHCA treatment, which results in a 24% increase of APAF1 protein levels. The intrinsic apoptotic

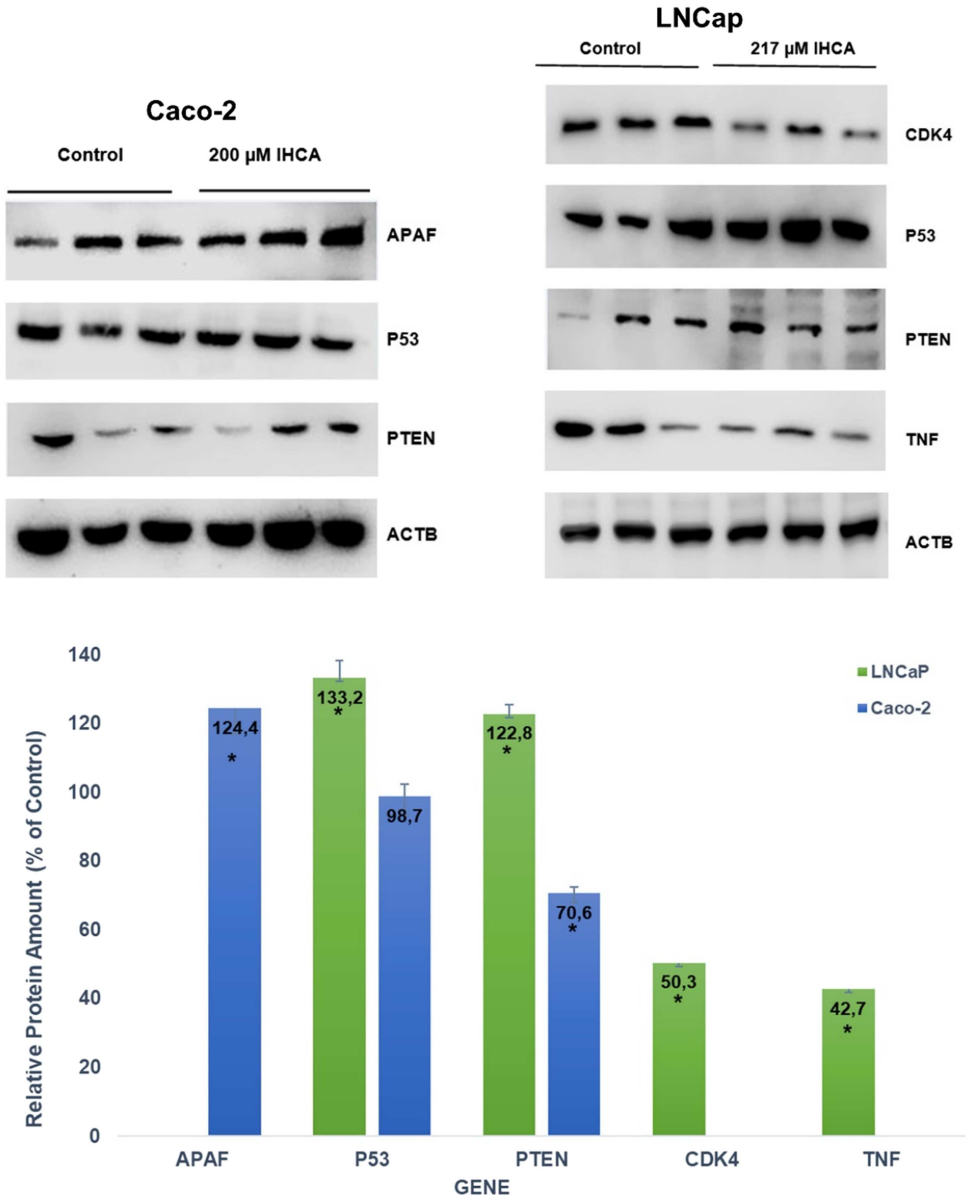

FIGURE 3 | Quantification of proteins in LNCaP and Caco-2 cells. The proteins were separated by SDS–PAGE, and western blot analysis was performed as described. Proteins were detected using the chemoluminescent substrate and quantitated using Scion Image Version 4.0.2 software. All values were normalized according to ACTB, and control values were taken as 100%. *Statistically significantly different than the control ($p < 0.05$).

pathway becomes active because APAF1 protein levels increase by 24% after IHCA treatment. The PTEN protein level decreases by 30% despite the fivefold increase in PTEN mRNA expression following IHCA treatment. The results demonstrate that PTEN undergoes strong post-transcriptional and post-translational control when Caco-2 cells receive IHCA treatment. The results indicate that IHCA affects tumor suppressor pathways differently between prostate and colorectal cancer cell lines.

2.5 | Measurement of Apoptosis Rates of LNCaP and Caco2 Cells

The examination of LNCaP and Caco-2 cell apoptosis with Annexin V/PI double staining revealed that following 24 h of treatment with the EC_{50} dose of IHCA, the apoptosis rates were $4.9 \pm 0.85\%$ and $42.5 \pm 5.32\%$, respectively. The apoptotic rate for the untreated control cells was $4.3 \pm 0.76\%$ and 5.2%. Furthermore, a statistically significant difference in the rate of apoptosis was seen when comparing the untreated control group with IHCA-treated LNCaP cells. Marked elevations in apoptosis rates were observed in the LNCaP cells relative to the Caco-2 cells ($p < 0.05$). A dosage of 217 μM ICHA caused apoptosis in LNCaP cells (Figure 4b). Comparable apoptotic effects were reported for indole-3-carbinol and its derivatives [70–72]. Alongside Annexin V/PI labeling, Casp3 protein levels were also quantified in LNCaP and Caco-2 cells subjected to the EC_{50} dose of IHCA, utilizing western blotting. A statistically significant and twofold rise in Casp3 protein levels was seen in LNCaP cells, concurrent with Annexin V/PI staining (Figure 4a). Statistically significant increases were observed in Caco-2 cells, albeit at a modest level of 1.15-fold. In summary, both Annexin V/P1 staining and Casp3 protein level assessments validate that IHCA promotes apoptosis, particularly in LNCaP cells.

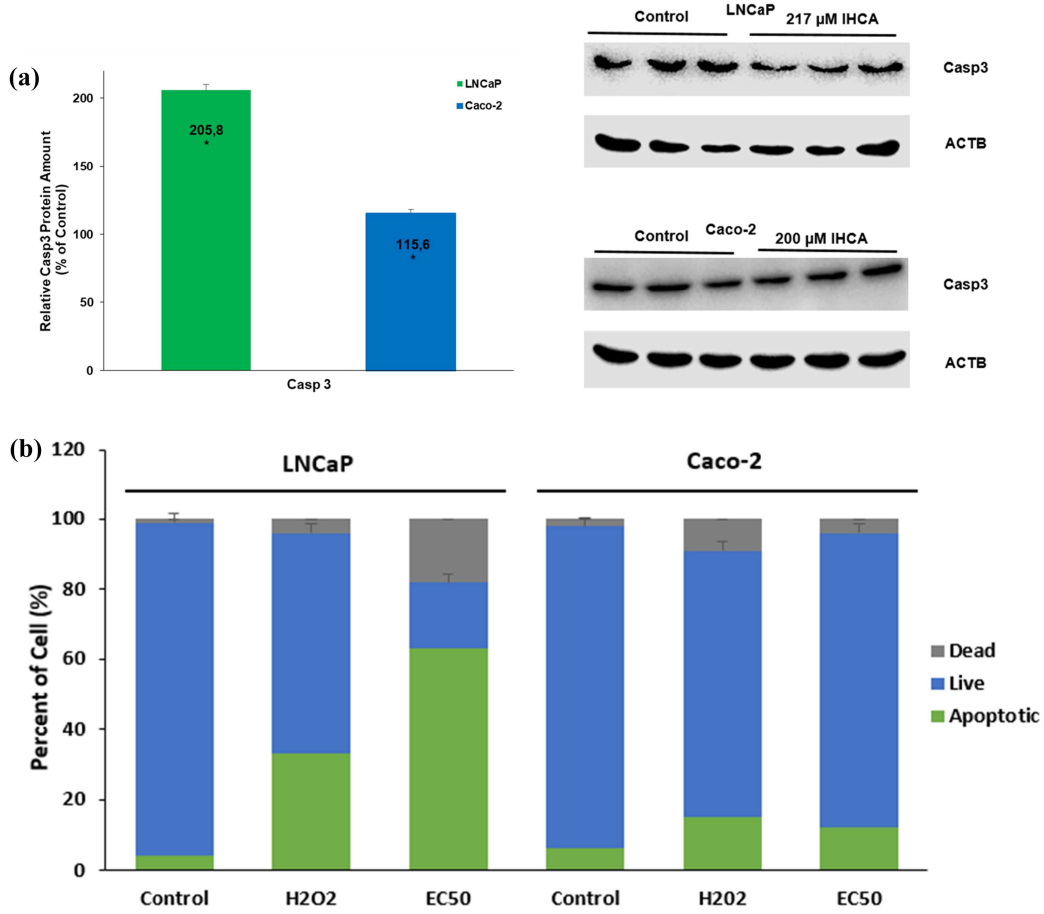

FIGURE 4 | (a) Quantification of Casp3 protein in LNCaP and Caco-2 cells. The proteins were separated by SDS–PAGE, and western blot analysis was performed as described. Proteins were detected using the chemoluminescent substrate and quantitated using Scion Image Version 4.0.2 software. All values were normalized according to ACTB, and control values were taken as 100%. *Statistically significantly different than the control ($p < 0.05$). (b) Apoptosis tests were performed using an image-based cytometer with an Annexin V/FITC/PI kit. Following a 24 h incubation period with IHCA, cells were assessed for apoptosis. H_2O_2 was used as a positive control (0.4 mM H_2O_2 for LNCaP cells and 0.5 mM H_2O_2 for Caco-2 cells).

The results from Annexin V/PI analysis match the previous findings about apoptotic gene expression. The IHCA treatment resulted in Caco-2 cells that experienced a 42.5% increase in apoptosis through the activation of the intrinsic apoptotic pathway, which was confirmed by APAF1 and CASP9 and CASP3 mRNA elevation and BCL2 mRNA reduction. The apoptosis level in LNCaP cells increased by a small amount from 4.3% to 4.9%, which corresponds to the limited changes in apoptotic gene expression. The Western blot analysis of Casp3 protein showed that Caco-2 cells experienced major apoptosis through elevated Casp3 protein levels (1.15-fold), but LNCaP cells showed a two-fold Casp3 protein increase without displaying Annexin staining. The treatment of Caco-2 cells with IHCA leads to effective apoptosis execution, but LNCaP cells show mostly gene expression changes.

2.6 | Effect of IHCA on the Transcriptional Activity of the P53 Promoter-Based Reporter Gene Assay

To further verify the effect of IHCA P53, transcriptional activity was measured by the luciferase reporter assay. For this purpose, HEK-293 cells transfected with the luc2P/P53 RE/Hygro plasmid containing two copies of a P53 response element (P53 RE) were treated with doxorubicin (as a positive control; i.e., a type of chemotherapy drug known to activate P53) and IHCA for 24 h. Then, the luciferase activities were measured. Doxorubicin treatment increased the luciferase activity 1.2-fold, while IHCA treatment at the EC_{50} dose caused a 1.7-fold induction in luciferase activity compared to the control (Figure 5).

The reporter gene assay further substantiated the P53-mediated apoptotic effect of IHCA observed at the gene and protein expression levels. To test the transcriptional susceptibility of P53 to the compounds tested, a reporter plasmid containing two copies of the P53 response element was transfected into HEK-293T cells. Reporter levels were then measured compared to the control chemotherapeutic agent doxorubicin, which is known to activate P53 transcriptionally [73]. The p53 reporter assay confirms the gene-expression results, which show IHCA activates the p53 signaling pathway. The results depict that IHCA causes P53 protein to build up while making its transcriptional function more powerful. The observation that IHCA stimulated reporter luciferase activity by approximately 20% more than doxorubicin indicates that it regulates P53 transcriptional activity positively.

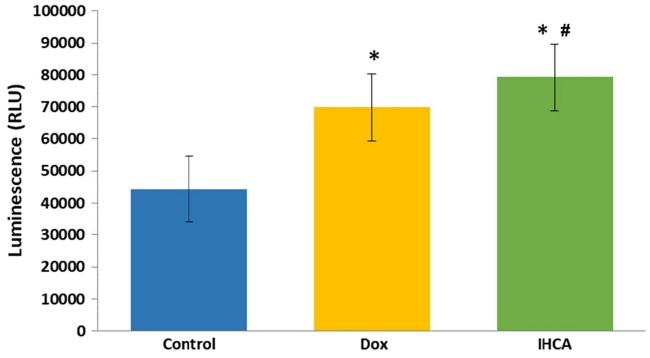

FIGURE 5 | HEK-293 cells transfected with luc2P/P53 RE/Hygro plasmid containing two copies of a P53 RE. Treatment with IHCA and doxorubicin for 24 h increased luciferase activities, as measured using the Dual-Glo Luciferase assay system. *Significantly different from the respective control value ($p < 0.05$). #; Significantly different from the respective doxorubicin value ($p < 0.05$).

2.7 | ADME Prediction

ADME (Absorption, Distribution, Metabolism, and Excretion) prediction is essential in drug design to assess a compound's pharmacokinetic properties. It helps optimize bioavailability, efficacy, and safety by predicting how a drug is absorbed, distributed, metabolized, and excreted in the body [74–77]. Early ADME predictions enhance the likelihood of clinical success by selecting compounds with favorable pharmacokinetic profiles. In this study, the ADME prediction of IHCA is provided in Table 2.

The ADME predictions for IHCA suggest that the compound exhibits favorable drug-like properties with respect to molecular weight *(177.16 g/mol)*, three hydrogen bond donors and four acceptors, lipophilicity *(QPlogPo/w: 2.250)*, and aqueous solubility (QPlogS: −2.379), all of which fall within acceptable ranges. Additionally, IHCA shows no violations of Lipinski's rule of five or Jorgensen's rule of three, confirming its compliance with drug-likeness criteria. However, the compound demonstrates moderate Caco-2 *(QPPCaco: 55)* and MDCK *(QPPMDCK: 27)* permeability, indicating room for improvement in bioavailability. Similarly, the human oral absorption *(% HOA: 71%)* is moderate. The brain/blood partitioning *(QPlogBB: −0.944)* suggests limited CNS penetration, which may or may not align with the compound's therapeutic purpose. The in silico ADME analysis indicates IHCA demonstrates standard permeability and oral absorption characteristics because of its polar structure, which contains ionized groups (phenolic OH and acidic carboxylate) that need optimization through rational design. The first practical method for development involves making prodrug esters from the 3-carboxylic acid and 2-hydroxy groups to enhance lipophilicity and reduce ionization through basic alkyl esters or amino acid promoieties, which enzymes in the intestine and liver can convert into their original structures. The addition of small hydrophobic groups to the indole ring through 5-methyl or 5-halogen or 5-CF_3 substituents helps the compound penetrate membranes better while preserving the 2-hydroxy/3-acid pharmacophore structure when solubility levels are managed correctly. The indole nitrogen accepts short "soft" alkyl chains or cleavable promoieties to change lipophilicity and metabolic stability, which produces soft prodrugs that convert into IHCA or an equivalent active compound. The proposed medicinal chemistry approach begins with basic ester and ring-substituted compounds to study permeability effects on biological responses before advancing to bioisosteric compounds that improve target binding and oral drug absorption. Overall, while IHCA displays promising pharmacokinetic properties, structural optimizations could focus on enhancing permeability and absorption to improve its drug-like potential further.

TABLE 2 | ADME prediction of IHCA.

ADME descriptor	IHCA	Reference values
Molecular weight	177.16	130.0 to 725.0
Donor Hydrogen bond	3	0.0 to 6.0
Accept Hydrogen bond	4	2.0 to 20.0
QPlogPo/w	2.250	−2.0 to 6.5
QPlogS	−2.379	−6.5 to 0.5
QPPCaco	55	< 25 poor, > 500 great
QPlogBB	−0.944	−3.0 to 1.2
QPPMDCK	27	< 25 poor, > 500 great
% Human oral a absorption	71	0%–100%, > 80% high, < 25% poor
Rule of five	0	Max violations 4
Rule of Three	0	Max violations 3

2.8 | Molecular Docking Studies

To complement and extend our in vitro findings, we next sought to determine whether the observed activation of P53 signaling and modulation of apoptotic pathways by IHCA could be rationalized at the molecular level. Specifically, because our gene and protein expression data pointed to a P53-centred mechanism and suggested possible interference with negative regulators such as MDM2, we turned to in silico approaches. We therefore performed molecular docking and molecular dynamics (MD) simulations to examine the binding mode, stability, and predicted affinity of IHCA within the MDM2 pocket, and to compare its behavior with that of reference ligands.

Molecular docking is a computational technique used to predict the interaction between a small molecule (ligand) and a target protein and possible inhibition mechanism, playing a crucial role in drug design. By simulating how a ligand fits into the binding site of a protein, molecular docking provides insights into the binding affinity and orientation of the ligand, which are essential for evaluating its potential as a drug candidate. To enhance accuracy, Induced Fit Docking (IFD) is employed, allowing both the ligand and the protein to adjust their conformations during binding. This flexibility is particularly important when significant structural changes occur, leading to a more realistic prediction of the binding mode. On the other hand, MM-GBSA (Molecular Mechanics/Generalized Born Surface Area) calculations are often used to estimate the binding free energy, offering a more detailed assessment of the

ligand's thermodynamic stability within the protein's active site. Together, these techniques provide a comprehensive framework for understanding the interactions between drugs and their targets, optimizing lead compounds, and guiding the design of molecules with improved specificity and efficacy in drug discovery [78]. In this study, IFD was performed to determine the ligand-protein interaction between IHCA and MDM2 protein. In addition, MM-GBSA ΔG binding free energies were calculated for both IHCA and reference drug nutlin-3a. The IFD docking scores and MM-GBSA ΔG binding free energies of IHCA and Nutlin-3a are given in Table 3.

The results, as shown in Table 3, reveal that IHCA exhibits a significantly better IFD XP Glide score of −8.166 kcal/mol compared to Nutlin-3a′s −4.730 kcal/mol. This indicates a stronger predicted binding affinity of IHCA to the MDM2 protein. Furthermore, the MM-GBSA ΔG binding free energy for IHCA is markedly more favorable at −60.98 kcal/mol, compared to −29.52 kcal/mol for Nutlin-3a, suggesting that IHCA forms a more thermodynamically stable complex with MDM2.

These findings highlight the potential of IHCA as a potent MDM2 inhibitor, with both stronger binding affinity and more excellent stability compared to the well-established Nutlin-3a. The superior IFD scores and binding free energies emphasize IHCA's promise as a lead compound in the development of new anticancer therapies targeting the MDM2 protein.

The molecular docking ligand protein interactions of both IHCA-MDM2 and Nutlin-3a-MDM2 complexes are given in Figures 6 and 7, respectively.

Figure 6a represents the 2D ligand protein interactions between IHCA and MDM2. As seen in Figure 6a, the hydroxyl group of IHCA formed a hydrogen bond interaction (purple arrow) with His-96. Moreover, there are two different hydrogen bond interactions. While the hydrogen atom of indole nitrogen formed a hydrogen bond with Val-93, the hydroxyl group of carboxylic acid moiety interacted with Leu-54. These polar interactions are essential for the specificity and strength of the binding. In addition to these strong polar hydrogen bond interactions, two π-π stacking hydrophobic interactions (green lines) are observed between the IHCA and the active site of the protein. The pyrrole ring of IHCA interacted with His-96, while the benzene ring interacted with Phe-91 via π-π stacking interactions. These π-π stacking interactions are crucial for enhancing the overall binding stability and affinity of IHCA to MDM2.

Figure 6b represents the 3D ligand protein interactions between IHCA and MDM2. In Figure 6b, while the yellow dashes depict the hydrogen bonds, the turquoise dashes represent the π-π stacking interactions. As seen in Figure 6b, IHCA has a planar rigid structure. For this reason, it can easily stack with amino acid residues in the active site of the enzyme. With its small structure, it interacts closely with many amino acid residues in the active site of the enzyme, and its hydrogen bond lengths vary between 1.82 Å and 2.30 Å.

Figure 7 represents the ligand-protein interactions between reference drug Nutlin-3a and MDM2. As seen in Figure 7a, there is only one interaction between Nutlin-3a and the active site of MDM2. His-96 formed a π-π stacking interaction with the chlorinated phenyl ring of Nutlin-3a. As can be seen from the 3D structure of Nutlin-3a **(**Figure 7b**),** the parts of the molecule are folded over each other and are away from the amino acids in the active site of the enzyme. This situation is also clearly seen in the surface binding analysis **(**Figure 8**).** As a result, IHCA seems to have a better potential than the reference drug. When looked at mechanistically, both molecules use the His-96 amino acid residue in common. In IHCA, four different interactions are observed with three different additional amino acids, which makes it a better inhibitor candidate.

Molecular docking 3D surface binding analysis of both compounds with the active site of the MDM2 is given in Figure 8. As can be seen from Figure 8, while IHCA completely fits into the binding site of the enzyme, a part of Nutlin-3a remains outside the binding surface area. This difference in binding behavior suggests that IHCA has superior conformational compatibility with the MDM2 active site, which may contribute to its stronger binding affinity and more stable interaction, as previously observed in the docking scores and binding free energy analyses. The ability of IHCA to fully occupy the binding site enhances its potential as a more effective MDM2 inhibitor compared to Nutlin-3a, further emphasizing its promise as a lead compound for anticancer drug development targeting the MDM2 protein.

As a result, molecular docking analyses revealed that IHCA demonstrates superior binding potential to the MDM2 protein compared to Nutlin-3a. The IFD docking scores and MM-GBSA ΔG binding free energies indicate that IHCA has a more favorable binding profile, with an IFD XP Glide score of −8.166 kcal/mol and an MM-GBSA ΔG binding free energy of −60.98 kcal/mol, in contrast to Nutlin-3a′s −4.730 kcal/mol and −29.52 kcal/mol, respectively. Figures 6 and 7 show that IHCA establishes multiple hydrogen bonds and π-π stacking interactions with various amino acids in the MDM2 active site, enhancing its binding stability and specificity. Conversely, Nutlin-3a exhibits a less optimal fit, with only partial occupancy of the binding site. Figure 8 further demonstrates that IHCA fully occupies the binding site, suggesting superior conformational compatibility and a stronger binding affinity. Overall, these findings highlight IHCA's potential as a more effective MDM2 inhibitor compared to Nutlin-3a, positioning it as a promising lead compound for anticancer drug development targeting MDM2.

TABLE 3 | Molecular docking scores and MM-GBSA ΔG binding free energies of IHCA and reference drug against MDM2 (PDB ID: 4HG7).

MDM2 (PDB ID: 4HG7)	IHCA	Nutlin-3a
IFD XP Glide Scores (kcal/mol)	−8.166	−4.730
MM-GBSA ΔG Binding Free Energies (kcal/mol)	−60.98	−29.52

2.9 | Molecular Dynamics

Molecular dynamics (MD) simulations are vital in drug discovery to assess the stability and flexibility of protein-ligand complexes. Two critical parameters in these simulations are Root Mean Square Deviation (RMSD) and Root Mean Square Fluctuation (RMSF). RMSD measures the average deviation of atomic

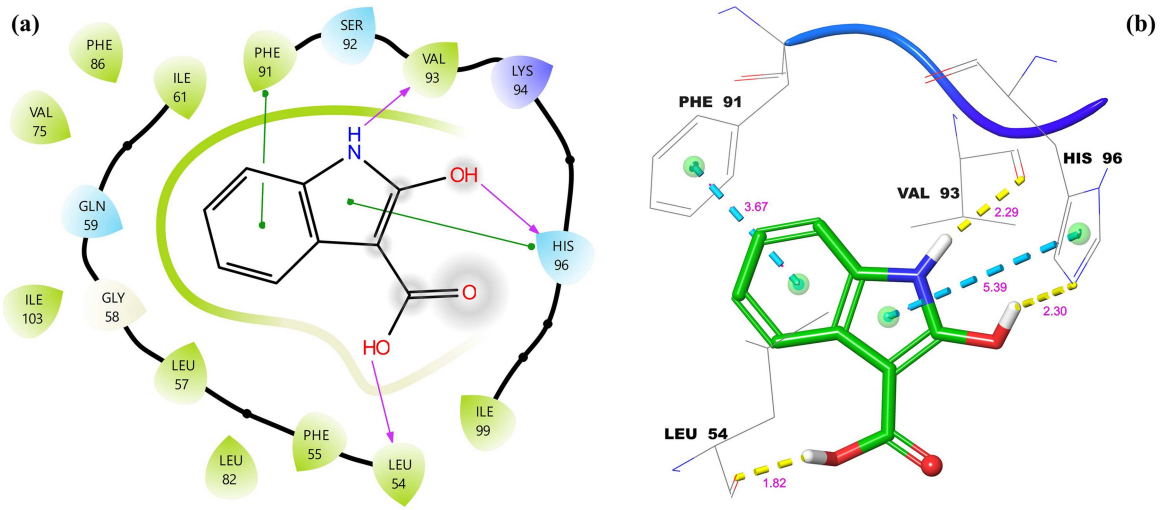

FIGURE 6 | Molecular docking 2D (a) and 3D (b) ligand protein interactions between IHCA and active site of MDM2.

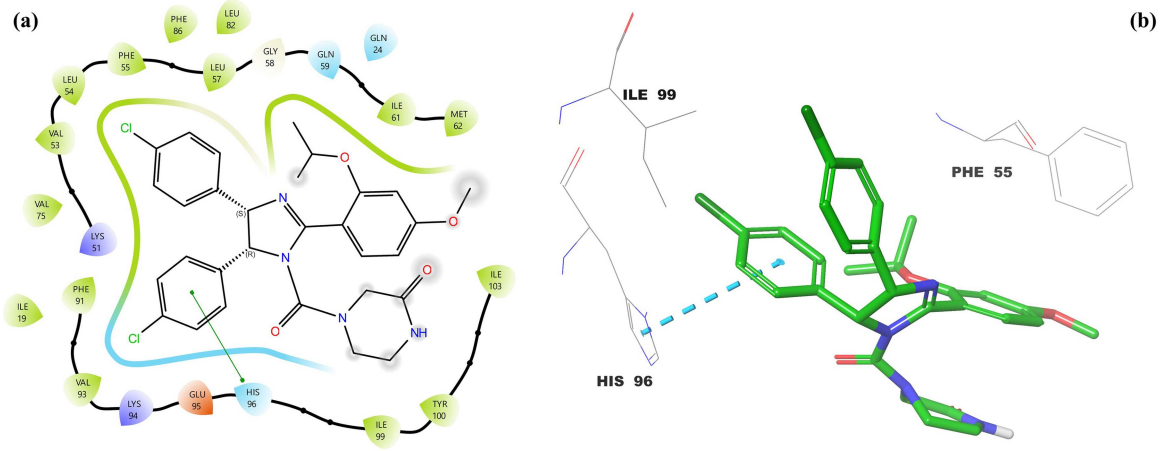

FIGURE 7 | Molecular docking 2D (a) and 3D (b) ligand protein interactions between Nutlin-3a and active site of MDM2.

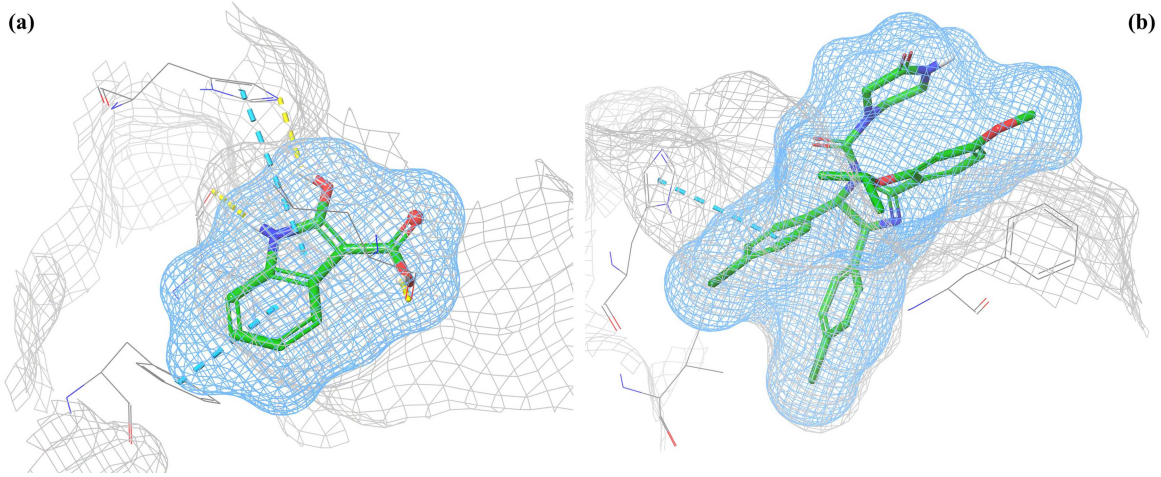

FIGURE 8 | Molecular docking 3D surface binding analysis of both IHCA (a) and Nutlin-3a (b) in the active site of MDM2.

positions from a reference structure, helping evaluate the stability of the ligand within the protein's binding site. A low RMSD indicates stable binding, while a high RMSD suggests potential instability or weak interactions. RMSF, on the other hand, quantifies the fluctuation of individual residues relative to their average positions, providing insights into the flexibility and dynamics of specific regions. High RMSF values in certain residues can signal increased mobility, which may impact binding

stability and efficacy. Together, RMSD and RMSF offer a comprehensive view of the stability and dynamics of ligand-protein interactions, guiding the optimization of drug candidates and the understanding of their mechanisms of action [79–81].

The 100 ns MD simulation analysis of the **IHCA-MDM2** complex, depicted in Figure 9, provides valuable insights into the binding interactions and stability of the complex. Figure 9a illustrates the key ligand-protein interactions throughout the simulation. The indole nitrogen of IHCA forms both a direct hydrogen bond and a water-bridged hydrogen bond with Leu-54, accounting for 31% and 10% of the simulation time, respectively. The hydroxyl group of the carboxylic acid moiety engages in two distinct water-bridged hydrogen bond interactions with Gln-72 (53% of the simulation time) and Val-93 (12% of the simulation time), highlighting the important role of these interactions in maintaining the stability of the **IHCA-MDM2** binding. IHCA also has two intramolecular hydrogen bond interactions between its hydroxyl and carboxylic acid groups. These happen 22% and 19% of the time during the simulation, which makes its structure even more stable. The pyrrole ring of IHCA also forms a π-π stacking interaction with His-96 for 13% of the simulation time, adding to the overall stability of the binding interaction.

Figure 9b presents the RMSD analysis of protein and ligand atoms from the 100 ns MD simulation of the **IHCA-MDM2** complex. The average RMSD of protein Cα atoms is 1.12 Å, indicating a relatively stable protein structure throughout the simulation. In contrast, the average RMSD of ligand atoms is 3.15 Å, reflecting a higher degree of deviation from the initial binding pose. This suggests that the ligand experiences more

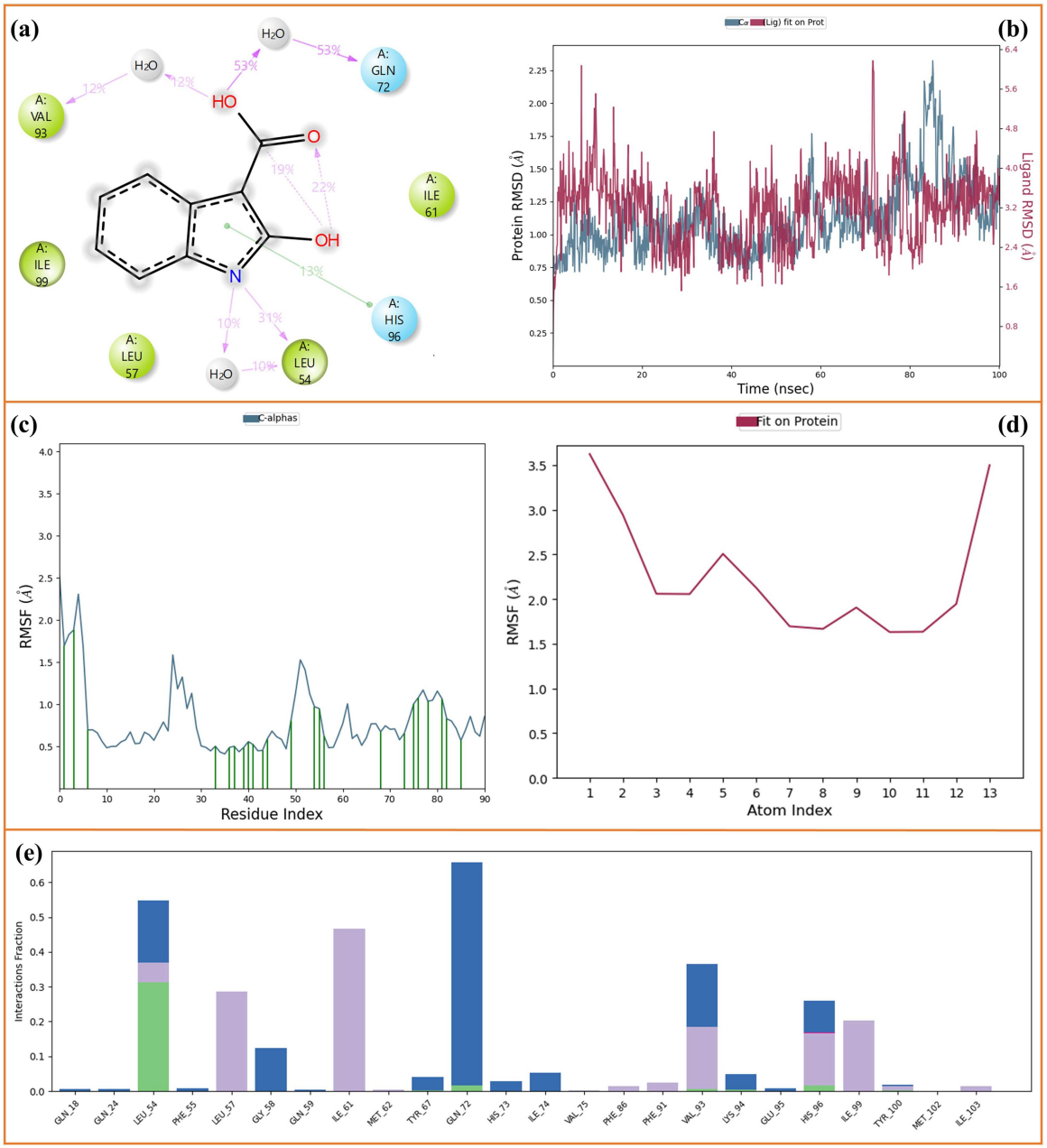

FIGURE 9 | The 100 ns MD simulation analysis of IHCA-MDM2 complex. (a) 2D key ligand-protein interactions, (b) RMSD of ligand and protein atoms, (c) RMSF of protein atoms, (d) RMSF of ligand atoms, (e) fractional interaction histogram.

significant conformational changes or fluctuations during the simulation. Additionally, the average deviation of the ligand from its original position is 0.51 Å, which highlights that while there are some positional shifts, the ligand remains relatively close to its initial binding site.

Figures 9c and 9d provide insights into the flexibility of the IHCA-MDM2 complex by showing the RMSF of protein Cα atoms and ligand atoms, respectively. In Figure 9c, the average RMSF of protein Cα atoms is 0.81 Å, indicating relatively low flexibility of the protein throughout the simulation. This suggests that the protein structure is stable, with minimal fluctuations in the residues, which is crucial for maintaining the integrity of the binding site. In Figure 9d, the ligand atoms exhibit an average RMSF of 2.25 Å, indicating greater flexibility compared to the protein. This higher RMSF value reflects that the ligand undergoes more substantial fluctuations and movements during the simulation. The green vertical lines in Figure 9c highlight the contact points between the ligand and specific amino acids in the protein, suggesting that regions of the protein directly interacting with the ligand might be more stable while the ligand itself remains more dynamic [75].

Figure 9e represents the fractional interaction histograms of the IHCA-MDM2 complex during 100 ns simulation time. In an MD simulation, the interactions between amino acid residues and functional groups over the simulation period are cumulatively collected to generate the total fractional interaction histogram. A functional group can simultaneously interact with multiple amino acids, and likewise, a single amino acid residue can engage in various types of interactions with different functional groups. In Figure 9e, the green columns represent hydrogen bond interactions, the blue columns indicate water-bridged hydrogen bond interactions, and the purple columns depict hydrophobic π-π stacking interactions. According to Figure 9e, the most abundant fractional interactions were observed with Gln-72, Leu-54, Ile-61 Val-93 and His-96. In conclusion, the 100-nanosecond MD simulation of the IHCA-MDM2 complex reveals critical binding interactions and stability factors. IHCA forms hydrogen bonds with Leu-54 and water-bridged hydrogen bonds with Gln-72 and Val-93. It also shows intramolecular hydrogen bonds and a π-π stacking interaction with His-96. The protein and ligand remain stable. Frequent interactions occur with Gln-72, Leu-54, Ile-61, Val-93, and His-96. These findings highlight key residues and functional groups that contribute to the stability and potential for effective MDM2 inhibition.

To verify the MD simulation results and calculate standard deviations, the MD simulation of the **IHCA-MDM2** ligand-protein complex was performed in triplicate using random seed. RMSD and RMSF graphs obtained from the random seed MD simulation analysis are given in Figure 10 as combined. In addition, the average values of the RMSD and RMSF graphs obtained from the random seed MD simulations are given in Figure 10, and the comparison of these values with the custom seed is given in Table 4.

The MD simulation results indicate that the custom seed generally provides a more stable and consistent simulation for the **IHCA-MDM2** complex compared to the average random seeds. The RMSD values for Protein Cα Atoms (1.12 vs. 1.27), Protein Backbone (1.13 vs. 1.27), and Ligand fit on Protein (3.15 vs. 3.64) are lower with the custom seed, suggesting better stability in these regions. In contrast, the RMSD for Ligand fit on Ligand is very similar between the custom seed and random seeds (0.51 vs. 0.49), indicating comparable consistency in ligand conformation. The RMSF values, reflecting flexibility, are also close between the two methods. For Protein Cα Atoms and Protein Backbone, the custom seed values are slightly higher (0.81 vs 0.79 and 0.82 vs 0.80, respectively), while the RMSF for Ligand Atoms is lower with the custom seed (2.25 vs 2.58), indicating less fluctuation and a more stable ligand position. These findings validate the custom seed analysis against the random seed analyses, confirming the reliability of the results.

3 | Conclusions

In conclusion, this study provides compelling evidence for the anticancer potential of the natural small indole derivative IHCA derived from *Capparis ovata*. IHCA effectively modulates key apoptotic and tumor suppressor genes, particularly enhancing the expression of P53 and PTEN while downregulating oncogenic markers such as KRAS in prostate (LNCaP) and colorectal (Caco-2) cancer cells. IHCA operates tumor defense mechanisms to trigger programmed cell death, activating p53, PTEN and RB proteins through APAF1–caspase-9–caspase-3 apoptosis pathway, which results in mitochondrial apoptosis instead of inflammation because it reduces BCL2 levels and blocks TNF production. Western blot and luciferase assays further support its role in activating the P53 signaling pathway. Molecular docking and molecular dynamics (MD) simulations revealed that IHCA exhibits strong and stable binding to the MDM2 protein, surpassing even the reference compound Nutlin-3a in interaction stability. The direct comparison of binding modes demonstrates that IHCA interacts with a broader set of key MDM2 residues, including Leu-54, Gln-72, Ile-61, Val-93, and His-96, through multiple hydrogen bonds, water-bridged interactions, and π–π stacking, resulting in superior docking scores, more favorable MM-GBSA binding free energy, and enhanced MD stability. In contrast, Nutlin-3a forms only a single π–π stacking interaction and shows limited pocket occupancy. Additionally, its selective mechanism of action underscores its potential as a safe and promising lead compound for the development of novel anticancer therapeutics or combination therapies that activate multiple tumor suppressor pathways while minimizing TNF-induced inflammation.

4 | Experimental

4.1 | Chemicals and Reagents

The solvents hexane, dichloromethane, ethanol, methanol, silica gel 60 (0.063–0.200 mm) for column chromatography and TLC silica gel 60 F254 plates were purchased from Merck (Darmstadt, Germany). Bovine serum albumin (BSA), bicinchoninic acid (BCA), glycine, Dulbecco's modified Eagle's medium (DMEM), Roswell Park Memorial Institute 1640 medium (RPMI), fetal bovine serum (FBS), trypsin, penicillin/streptomycin mixture, sodium dodecyl sulfate (SDS) and 2-amino-2-(hydroxymethyl) −1,3-propanediol (TRIS) were purchased from Sigma–Aldrich Chemical Company (St Louis, Missouri, USA). Antibodies against PTEN, P53, APAF, ACTB, CDK4, TNF and secondary antibodies were purchased from Abcam (Abcam PLC, Cambridge, UK). An Easy Script cDNA Synthesis Kit and SYBR Green qPCR master

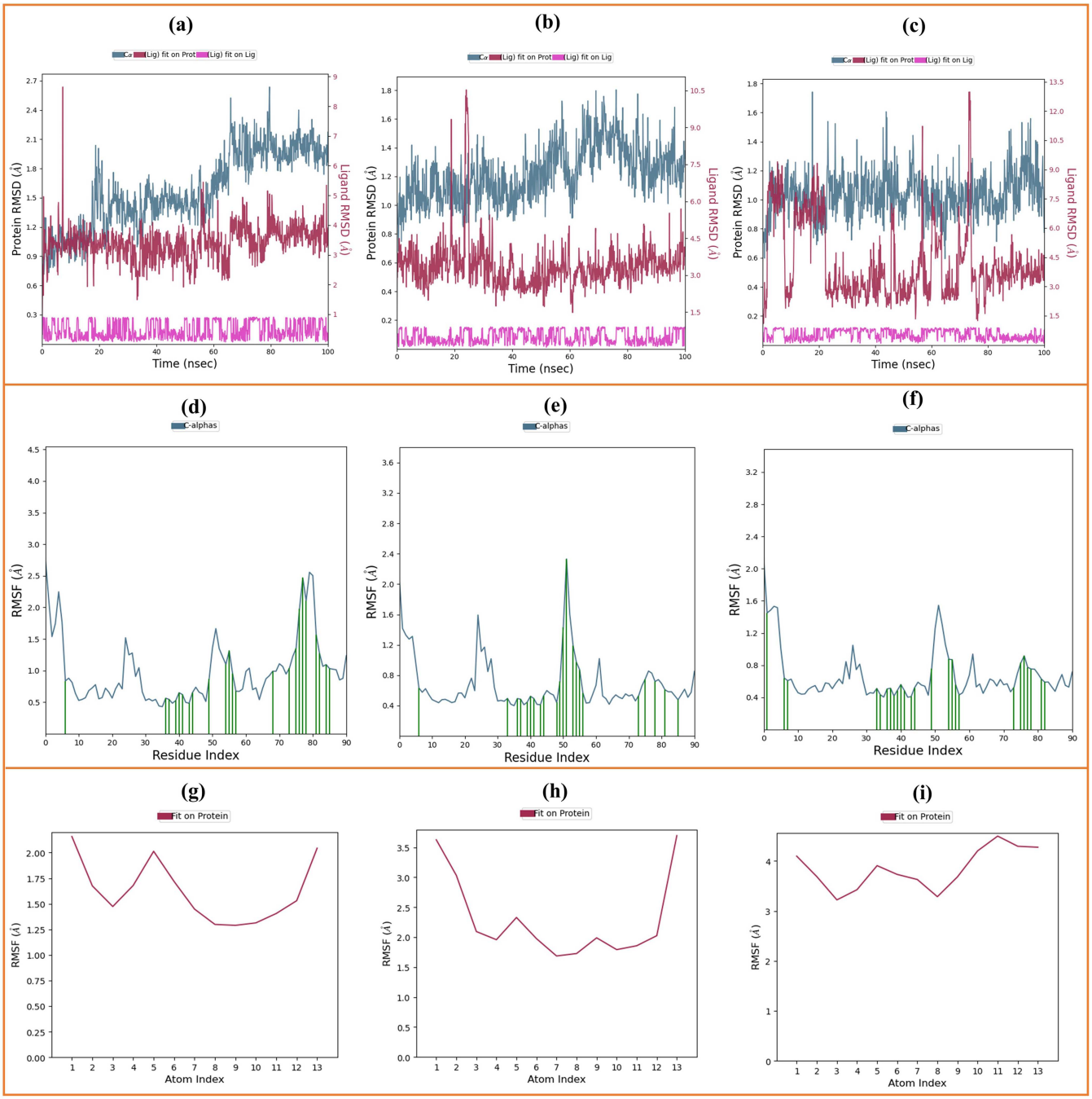

FIGURE 10 | In triplicate Random Seed (RS) MD simulation analysis of **IHCA-MDM2** complex. (a) RMSD of protein and ligand atoms for RS1, (b) RMSD of protein and ligand atoms for RS2, (c) RMSD of protein and ligand atoms for RS3, (d) RMSF of protein atoms for RS1, (e) RMSF of protein atoms for RS2, (f) RMSF of protein atoms for RS3, (g) RMSF of ligand atoms for RS1, (h) RMSF of ligand atoms for RS2, (i) RMSF of ligand atoms for RS3.

mix were purchased from Applied Biological Materials Inc. (ABM; Richmond, Canada). All other chemicals and solvents were obtained from commercial sources at the highest grade of purity available.

4.2 | Cell Cultures and Cell Proliferation Assay

The human prostatic adenocarcinoma cell line (LNCaP), colorectal adenocarcinoma cell lines (Caco-2) and human embryonic kidney 293 T (HEK-293T) cells were obtained from the American Type Culture Collection (ATCC, USA). The cells were cultured in RPMI and DMEM supplemented with 10% FBS and a 1% penicillin/streptomycin mixture in a humidified atmosphere of 95% air with 5% CO_2 at 37°C and sub-cultured twice a week. Cell viability was assessed as previously described [82]. Briefly, LNCaP and Caco-2 cells were seeded in 96-well plates at a density of 1×10^3 cells/mL culture medium. After 24 h of incubation, the cells were treated with varying concentrations of IHCA (ranging from 10 μM to 200 μM) and the control drug Taxol (ranging from 1 nM to 50 nM). The IHCA-treated, Taxol-treated and control cells were incubated for an

TABLE 4 | MD Simulation custom and random seed average RMSD and RMSF values of protein and ligand atoms of IHCA-MDM2 complex.

	Random seed 1	Random seed 2	Random seed 3	Average of random seeds	Custom seed
RMSD of protein Cα atoms	1.57	1.22	1.03	1.27	1.12
RMSD of protein backbone	1.55	1.21	1.05	1.27	1.13
RMSD of ligand fit on protein	3.41	3.36	4.14	3.64	3.15
RMSD of ligand fit on ligand	0.46	0.48	0.54	0.49	0.51
RMSF of protein Cα atoms	1.00	0.69	0.67	0.79	0.81
RMSF of protein backbone	1.00	0.71	0.69	0.80	0.82
RMSF of ligand atoms	1.61	2.29	3.84	2.58	2.25

TABLE 5 | Primer sequences of the selected human genes.

Gene bank accession number	Gene	Sense primer (5′- > 3′)	Antisense primer(5′- > 3′)	Tm (°C)
NM_181861	APAF1	GTCTGCTGATGGTGCAAGGA	GATGGCCCGTGTGGATTTC	61
NM_001101	BACT	TCCTCCTGAGCGCAAGTACTC	CTGCTTGCTGATCCACATCTG	60.5
NM_138764	BAX	AGAGGATGATTGCCGCCGT	CAACCACCCTGGTCTTGGATC	57.5
NM_000633	BCL2	TGCACCTGACGCCCTTCAC	AGACAGCCAGGAGAAATCAAACAG	63
NM_004346	CASP3	GCAGCAAACCTCAGGGAAAC	TGTCGGCATACTGTTTCAGCA	61
NM_033358	CASP8	TCTGGAGCATCTGCTGTCTG	CCTGCCTGGTGTCTGAAGTT	59
NM_001229	CASP9	GGCTGTCTACGGCACAGATGGA	CTGGCTCGGGGTTACTGCCAG	61
NM_000075	CDK4	ATGTTGTCCGGCTGATGGA	CACCAGGGTTACCTTGATCTCC	59.5
NM_002467	c-MYC	TCCATGAGGAGACACCGCC	GCTGTGAGGAGGTTTGCTGT	62
NM_001759	CYCD2	TTCCGCAGTGCTCCTACTTC	CGCACTTCTGTTCCTCACAG	59.2
NM_152872	FAS	CACTTCGGAGGATTGCTCAACA	TATGTTGGCTCTTCAGCGCTA	60.5
NM_001369787	KRAS	CTCGACACAGCAGGTCAAGA	GGCATCATCAACACCCTGTC	59
NM_001276696	P53	ATCTACAAGCAGTCACAGCACAT	GTGGTACAGTCAGAGCCAACC	61
NM_000314	PTEN	CCCAGACATGACAGCCATC	TCTGCAGGAAATCCCATAGC	58.5
NM 000321	RB	ATCTATATTTCACCCCTGAAGAGTC	TTCAGAAGGTCTGCCAACACCAACA	59
NM_000594	TNF	GCCATTGGCCAGGAGGGC	CGCCACCACGCTCTTCTG	62

additional 24 h at 37°C in a humidified 5% CO_2 atmosphere. Following incubation, the medium was replaced by 0.5% crystal violet solution (w/v; in 50% ethanol). Dye absorbed by live cells was extracted with sodium citrate (0.1 M in 50% ethanol), and the absorbance was read at 630 nm. Viability was expressed as a percentage of the control cells.

4.3 | Real-Time Quantitative PCR for Gene Expression Analysis at the mRNA Level

Real-time PCR was performed as previously optimized [17]. RNA concentration was determined using a Nanodrop (MaestroNano microvolume Spectrophotometer, USA), and the RNA was reverse transcribed using an Easy Script cDNA Synthesis Kit (ABM). The reaction mixture was incubated for 50 min at 50°C, followed by termination by heating at 5 min at 85°C. cDNA was stored at −80°C for further use. Quantitative real-time PCR (qPCR) analysis was carried out using SYBR Green qPCR Master Mix (GM, Taiwan) in an Exicycler 96 Real-Time Quantitative Thermal Block PCR System (Bioneer, Daejeon, Korea) for each gene. The mRNA levels of genes (APAF1, BACT, BAX, BCL2, CASP3, CASP8, CASP9, CDK4, c-MYC, CYCD2, FAS, KRAS, P53, PTEN, RB and TNF-α) were determined by qPCR using beta-actin as the reference gene. Custom-designed primers used for qPCR are listed in Table 5.

4.4 | Immunoblot Analysis for Gene Expression Analysis at the Protein Level

Total protein was extracted from Caco-2 and LNCaP cells with Qiazol lysis reagent (Qiagen, USA), as Lee et al. described [83]. Protein concentration was determined by BCA assay. As described elsewhere, sodium dodecyl sulfate-

polyacrylamide gel electrophoresis (SDS–PAGE) and Western blotting were performed [84]. Briefly, 80 μg protein samples were separated on 4% stacking and 12% separating polyacrylamide gels using the discontinuous buffer system of Laemmli [85]. Proteins were transferred to a nitrocellulose membrane using a Transblot electrophoretic transfer cell (Bio-Rad) containing Tris-glycine buffer, pH 8.3, and methanol. The transfer was carried out at 4°C for 90 min at 90 V (at max 400 mA). Following the transfer, the membranes were blocked using 5% nonfat dry milk in TBST (20 mM Tris-HCl, pH 7.4, 400 mM NaCl and 0.1% (v/v) Tween 20) for 60 min and incubated with APAF, P53, PTEN, ACTB, CDK4 and TNF-α antibodies overnight at 4°C. The membranes were washed with TBST (3 × 5 min) and incubated with the secondary antibody (HRP-conjugated IgG). Proteins were detected using SuperSignal® West Pico Chemoluminescent Substrate (Pierce, Rockford, IL, USA), and bands were visualized and recorded using the Odyssey® Fc Imaging System (LI-COR). Protein bands were quantified using Scion Image Version Beta 4.0.2 software.

4.5 | Measurement of Apoptosis Rates of LNCaP and Caco2 Cells

The annexin V-FITC apoptosis detection Kit (E-CK-A211; Elabscience) was used to measure apoptosis. Briefly, LNCaP and Caco2 cells were seeded in 6-well plates (1×10^5 cells/well) and cultured overnight at 37°C. After incubation, the determined EC50 doses of IHCA were applied to LNCaP and Caco-2 cells. H_2O_2 (hydrogen peroxide) served as the positive control (0.4 mM H2O2 for LNCaP cells and 0.5 mM H2O2 for Caco-2 cells) [86]. After 24 h, the cells were collected and centrifuged (2000 × g, 5 min) at 4°C. Finally, 100 μL of 1X binding buffer, 1 μL of annexin V-FITC and 1 μL of PI Staining Solution were added to the cells and gently mixed. The cells were then incubated in the dark at room temperature for 15 min. Apoptotic testing was performed using a fluorescence cell counter (Arthur-NanoEntek) [87]. Three replicates for each sample were measured.

4.6 | P53 Promoter-Based Reporter Gene Assay-Luciferase Assay

To evaluate the effect of IHCA on the transcriptional activity of P53, human embryonic kidney 293 T (HEK-293T) cells were grown in DMEM supplemented with 10% FBS and a 1% penicillin/streptomycin mixture in a humidified atmosphere of 95% air with 5% CO_2 at 37°C. Before transfection, cells were seeded in 96-well plates at approximately 1×10^4 cells/well. After 24 h, cells were transfected with Fugene HD reagent (Promega) using the pGL4.38 [luc2P/P53 RE/Hygro] plasmid containing two copies of a P53 response element (P53 RE) that drives transcription of the luciferase reporter gene luc2P. An additional 24 h after transfection, cells were stimulated with IHCA and doxorubicin (positive control) was used. After 24 h of stimulation, the cellular lysate was assayed for luciferase and Renilla activities using the Dual-Glo luciferase assay system (Promega) as optimized previously [88]. Luminescence was measured using a Synergy HTX luminometer (BioTek). Luciferase activities were normalized to Renilla activities.

4.7 | Statistical Analysis

Statistical analyses were applied using the Minitab 13 statistical software package (Minitab Inc., State College, PA, USA). All results are expressed as the means, including their standard error of the mean (SEM). Comparisons between groups were performed using Student's *t*-test, and $p < 0.05$ was selected as the level required for statistical significance.

4.8 | Computational Studies

Molecular Docking studies were carried out by Schrödinger Molecular Modelling Software (2024-1) with Maestro (13.9) interface. MD simulations were carried out using Desmond (D. E. Shaw Research) with Maestro (13.5) interface.

4.8.1 | Preparation of Ligands and Proteins

The methods that our research group previously published were used to perform protein and ligand preparation [89]. The 3D X-ray crystallographic structures of the target proteins were obtained from the Protein Data Bank, accessible via the RCSB website (https://www.rcsb.org). In this study, MDM2 (PDB ID: 4HG7) was used to carry out all in silico studies. Careful preparation and refinement of these protein structures were carried out using the Protein Preparation Wizard module within Schrödinger Maestro 13.9.

4.8.2 | Glide Docking and Induced Fit Docking

The methods that our research group previously published were used to perform glide docking and induced fit docking. The ligands we prepared were subjected to docking into the respective receptors using the IFD protocol, part of the Schrödinger suite (Schrödinger Release 2024-1, Induced Fit Docking protocol, Glide, Schrödinger LLC, New York, NY). The center of the Glide grid was determined based on the native ligand's centroid, with the inner box side set at 25 Å, and the outer box side was automatically defined. 20 poses for each ligand were derived according to the standard IFD protocol, and each pose was docked with Glide XP docking sensitivity. Finally, IFD docking scores, representing the binding energy, were computed for each generated pose [90].

4.8.3 | Prime MM-GBSA Analysis

The methods that our research group previously published were used to perform prime MM-GBSA analysis. The free binding energy between the ligand and protein in the docked poses was calculated using the Prime MM-GBSA module within the Schrödinger suite 2024-1, following methods described in previous publications [91, 92]. Default parameters, such as the VSGB solvation model and the Minimize sampling method, were used in the MM/GBSA module. During the energy calculation, specific residues surrounding the receptor pocket were constrained to maintain flexible conformations.

4.8.4 | *Molecular Dynamics Simulations*

The methods that our research group previously published were used to perform molecular dynamics simulations [93]. The protein-ligand complex was built using the Desmond system builder and then placed in a simulation box with a 10 Å buffer zone. Water (Tip3p model) and NaCl (0.15 M) were added to neutralize the system. The OPLS3 force field was used for energy minimization. A 100 ns molecular dynamics simulation at 300 °K and 1 bar pressure was run with a 100 ps time step using Desmond. Interactions between the ligand and protein were analyzed, and RMSD values for protein Cα atoms and ligand-heavy atoms were calculated to assess stability during simulation time [94].

4.8.5 | *ADME Prediction*

The ADME properties of the compound were predicted using the QikProp module integrated within the Schrödinger suite (Schrödinger, 2024). QikProp is a computational tool designed to evaluate key pharmacokinetic and physicochemical parameters relevant to drug-likeness and bioavailability. The process involves the following steps: The chemical structure of the compound was drawn or imported into the Maestro interface. The structure was then subjected to energy minimization using the OPLS4 force field to ensure proper geometry and stability. The prepared structure was submitted to the QikProp module. The tool estimates over 50 ADME-related descriptors, including molecular weight (MW), hydrogen bond donors and acceptors (Donor HB and Accept HB), lipophilicity (QPlogPo/w), solubility (QPlogS), permeability (QPPCaco and QPPMDCK), brain-blood partition coefficient (QPlogBB), human oral absorption (%HOA), and violations of Lipinski's and Jorgensen's rules [95, 96].

Author Contributions

Özden Özgün Acar: investigation, writing – original draft, validation. **Işıl Gazioğlu:** investigation, validation. **Hatice Oruç:** investigation, validation. **Elif Kale:** investigation, validation. **Halil Şenol:** conceptualization, software, methodology, investigation, writing – review and editing. **Gülaçtı Topçu:** conceptualization, software, methodology, investigation, writing – review and editing. **Alaattin Şen:** conceptualization, software, methodology, investigation, writing – review and editing, funding.

Acknowledgments

The authors would like to thank the Scientific and Technological Research Council of Turkey [TUBITAK-112S187] and Pamukkale University (2017FEBE051) for funding the work.

Ethics Statement

The authors have nothing to report.

Consent

The authors have nothing to report.

Conflicts of Interest

The authors declare no conflicts of interest.

Data Availability Statement

All data generated or analyzed during this study are included in this published article and its supplementary information files. The data that support the findings of this study are available within the manuscript.

References

1. R. L. Siegel, K. D. Miller, H. E. Fuchs, and A. Jemal, "Cancer Statistics, 2022," *CA: A Cancer Journal for Clinicians* 72, no. 1 (2022): 7–33, https://doi.org/10.3322/caac.21708.

2. F. Bray, J. Ferlay, I. Soerjomataram, R. L. Siegel, L. A. Torre, and A. Jemal, "Global Cancer Statistics 2018: Globocan Estimates of Incidence and Mortality Worldwide for 36 Cancers in 185 Countries," *CA: A Cancer Journal for Clinicians* 68, no. 6 (2018): 394–424, https://doi.org/10.3322/caac.21492.

3. H. Şenol, M. Ghaffari-Moghaddam, Ş. Bulut, F. Akbaş, A. Köse, and G. Topçu, "Synthesis and Anticancer Activity of Novel Derivatives of α,β-unsaturated Ketones Based on Oleanolic Acid: In Vitro and In Silico Studies Against Prostate Cancer Cells," *Chemistry & Biodiversity* 20, no. 9 (2023): e202301089, https://doi.org/10.1002/cbdv.202301089.

4. F. S. Tokalı, H. Şenol, T. G. Katmerlikaya, A. Dağ, and K. Şendil, "Novel Thiosemicarbazone and thiazolidin-4-one Derivatives Containing Vanillin Core: Synthesis, Characterization, and Anticancer Activity Studies," *Journal of Heterocyclic Chemistry* 60, no. 4 (2023): 645–656, https://doi.org/10.1002/jhet.4619.

5. S. Nobili, D. Lippi, E. Witort, et al., "Natural Compounds for Cancer Treatment and Prevention," *Pharmacological Research* 59, no. 6 (2009): 365–378, https://doi.org/10.1016/j.phrs.2009.01.017.

6. D. Xu and Z. Xu, "Indole Alkaloids With Potential Anticancer Activity," *Current Topics in Medicinal Chemistry* 20, no. 21 (2020): 1938–1949, https://doi.org/10.2174/1568026620666200622150325.

7. X. Wang, M. Yan, Q. Wang, et al., "In Vitro Dna-Binding, Antioxidant and Anticancer Activity of indole-2-carboxylic Acid Dinuclear Copper (II) Complexes," *Molecules* 22, no. 1 (2017): 171, https://doi.org/10.3390/molecules22010171.

8. S. Chowdhary, I. Shalini, A. Arora, and V. Kumar, "A Mini Review on Isatin, an Anticancer Scaffold With Potential Activities Against Neglected Tropical Diseases," *Pharmaceuticals* 15, no. 5 (2022): 536, https://doi.org/10.3390/ph15050536.

9. B. W. Megna, P. R. Carney, M. Nukaya, P. Geiger, and G. D. Kennedy, "Indole-3-carbinol Induces Tumor Cell Death: Function Follows Form," *Journal of Surgical Research* 204, no. 1 (2016): 47–54, https://doi.org/10.1016/j.jss.2016.04.021.

10. H. Wu, X. Zhu, B. Li, et al., "Investigating the Binding Properties of DNA/BSA With Novel Indole Carboxylic Acid Complexes (M = Ni(II), Cd(II))–a Comparative Analysis. I," *Norg Chim Acta* 590 (2026): 122985, https://doi.org/10.1016/j.ica.2025.122985.

11. Y. Zhou, Y. Tang, Q. Luo, Y. Hu, and W. Peng, "Indole-3-carboxylic Acid Enhanced Anticancer Potency of Doxorubicin via Induction of Cellular Senescence in Colorectal Cells," *Acta Poloniae Pharmaceutica* 81 (2024): 109–121, https://doi.org/10.32383/appdr/178491.

12. Z. Batool, G. Ö. A. Toraman, F. Çakır, et al., "Dual Targeting of Neuroblastoma and Cholinesterase by Morpholino/Pyrrolidino-Sulfonyl-Indole Thiosemicarbazones: Synthesis, Characterization, Enzyme Inhibition, Cytotoxicity, Docking and Dynamics Studies," *Bioorganic Chemistry* 167 (2025): 109252, https://doi.org/10.1016/j.bioorg.2025.109252.

13. B. T. Sridhar, N. G. Yernale, R. S. Gani, N. Gupta, S. V. Ganachari, and B. S. Mathada, "Recent Development of Indole Derivatives for Anticancer Activities: A Concise Review," *Journal of the Indian Chemical Society* 101, no. 10 (2024): 101282, https://doi.org/10.1016/j.jics.2024.101282.

14. A. S. Elgubbi, A. Y. A. Alzahrani, E. A. E. El-Helw, and S. S. Shaban, "Facile Synthesis and Antioxidant Activity Screening of Some Novel

3-substituted Indole Derivatives," *Polycyclic Aromatic Compounds* 44, no. 3 (2024): 2032–2045, https://doi.org/10.1080/10406638.2023.2210729.

15. I. Mushtaq and A. Ahmed, "Synthesis of Biologically Active Sulfonamide-Based Indole Analogs: A Review," *Future Journal of Pharmaceutical Sciences* 9, no. 1 (2023): 46, https://doi.org/10.1186/s43094-023-00500-5.

16. R. Arslan, N. Bektas, and Y. Ozturk, "Antinociceptive Activity of Methanol Extract of Fruits of Capparis Ovata in Mice," *Journal of Ethnopharmacology* 131, no. 1 (2010): 28–32, https://doi.org/10.1016/j.jep.2010.05.060.

17. O. Ozgun-Acar, G. Celik-Turgut, I. Gazioglu, et al., "Capparis Ovata Treatment Suppresses Inflammatory Cytokine Expression and Ameliorates Experimental Allergic Encephalomyelitis Model of Multiple Sclerosis in C57BL/6 Mice," *Journal of Neuroimmunology* 298 (2016): 106–116, https://doi.org/10.1016/j.jneuroim.2016.07.010.

18. A. Panico, V. Cardile, F. Garufi, C. Puglia, F. Bonina, and G. Ronsisvalle, "Protective Effect of Capparis Spinosa on Chondrocytes," *Life Sciences* 77, no. 20 (2005): 2479–2488, https://doi.org/10.1016/j.lfs.2004.12.051.

19. A. Sen, G. Topcu, O. Ozgun, et al., "Anti-Neuroinflammatory Effect of Butanolic Subextract of Capparis Ovata Water Extract," *Journal of Neuroimmunology* 275 (2014): 172–173, https://doi.org/10.1016/j.jneuroim.2014.08.464.

20. N. Tlili, W. Elfalleh, E. Saadaoui, A. Khaldi, S. Triki, and N. Nasri, "The Caper (Capparis L.): Ethnopharmacology, Phytochemical and Pharmacological Properties," *Fitoterapia* 82, no. 2 (2011): 93–101, https://doi.org/10.1016/j.fitote.2010.09.006.

21. L. Tesoriere, D. Butera, C. Gentile, and M. A. Livrea, "Bioactive Components of Caper (Capparis spinosa L.) From Sicily and Antioxidant Effects in a Red Meat Simulated Gastric Digestion," *Journal of Agricultural and Food Chemistry* 55, no. 21 (2007): 8465–8471, https://doi.org/10.1021/jf0714113.

22. H. Senol, O. Ozgun-Acar, A. Dağ, et al., "Synthesis and Comprehensive In Vivo Activity Profiling of Olean-12-en-28-ol, 3β-Pentacosanoate in Experimental Autoimmune Encephalomyelitis: A Natural Remyelinating and Anti-Inflammatory Agent," *Journal of Natural Products* 86, no. 1 (2023): 103–118, https://doi.org/10.1021/acs.jnatprod.2c00798.

23. R. O. Bakr and M. H. El Bishbishy, "Profile of Bioactive Compounds of Capparis Spinosa Var. Aegyptiaca," *Revista Brasileira de Farmacognosia* 26, no. 4 (2016): 514–520, https://doi.org/10.1016/j.bjp.2016.04.001.

24. İ. Çaliş, A. Kuruüzüm, and P. Rüedi, "1H-indole-3-acetonitrile Glycosides From Capparis Spinosa Fruits," *Phytochemistry* 50, no. 7 (1999): 1205–1208, https://doi.org/10.1016/S0031-9422(98)00669-4.

25. İ. Çalış, A. Kuruüzüm-Uz, P. A. Lorenzetto, and P. Rüedi, "6S)-Hydroxy-3-oxo-α-ionol Glucosides From Capparis Spinosa Fruits," *Phytochemistry* 59, no. 4 (2002): 451–457, https://doi.org/10.1016/S0031-9422(01)00399-5.

26. T. Gull, F. Anwar, B. Sultana, M. A. C. Alcayde, and W. Nouman, "Capparis Species: A Potential Source of Bioactives," *Industrial Crops and Products* 67 (2015): 81–96, https://doi.org/10.1016/j.indcrop.2014.12.059.

27. P. V. Khang, S. D. Thuong, V. V. Nhuong, S. Shen, and L. Ma, "Two New Polycyclic Compounds and Cytotoxic Activities of Ethanol and Ethyl Acetate Extract of Leaves Ofcapparis Dongvanensis(Sy.) and Their Chemotaxonomic Significance," *Polycyclic Aromatic Compounds* 42, no. 6 (2022): 3717–3723, https://doi.org/10.1080/10406638.2020.1871383.

28. F. Mantovani, L. Collavin, and G. Del Sal, "Mutant p53 as a Guardian of the Cancer Cell," *Cell Death & Differentiation* 26, no. 2 (2019): 199–212, https://doi.org/10.1038/s41418-018-0246-9.

29. A. Hafner, M. L. Bulyk, A. Jambhekar, and G. Lahav, "The Multiple Mechanisms That Regulate p53 Activity and Cell Fate," *Nature Reviews Molecular Cell Biology* 20, no. 4 (2019): 199–210, https://doi.org/10.1038/s41580-019-0110-x.

30. A. Sen, G. Topcu, O. Ozgun, et al., "Anti-Neuroinflammatory Effect of Butanolic Subextract of Capparis Ovata Water Extract Used as an Alternative and Complementary Treatment for Multiple Sclerosis," *Journal of Neuroimmunology* 275 (2014): 172–173, https://doi.org/10.1016/j.jneuroim.2014.08.464.

31. B. Biersack and R. Schobert, "Eindole Compounds Against Breast Cancer: Recent Developments," *Current Drug Targets* 13, no. 14 (2012): 1705–1719, https://doi.org/10.2174/138945012804545551.

32. M. Chripkova, F. Zigo, and J. Mojzis, "Antiproliferative Effect of Indole Phytoalexins," *Molecules* 21 (2016): 1626.

33. R. Gaikwad, S. Ghorai, S. A. Amin, et al., "Monte Carlo Based Modelling Approach for Designing and Predicting Cytotoxicity of 2-phenylindole Derivatives Against Breast Cancer Cell Line Mcf7," *Toxicology In Vitro* 52 (2018): 23–32, https://doi.org/10.1016/j.tiv.2018.05.016.

34. J. G. Quirit, S. N. Lavrenov, K. Poindexter, et al., "Indole-3-carbinol (I3C) Analogues Are Potent Small Molecule Inhibitors of NEDD4-1 Ubiquitin Ligase Activity That Disrupt Proliferation of Human Melanoma Cells," *Biochemical Pharmacology* 127 (2017): 13–27, https://doi.org/10.1016/j.bcp.2016.12.007.

35. İ. Çaliş, A. Kuruüzüm, and P. Rüedi, "1H-indole-3-acetonitrile Glycosides From Capparis spinosa," *Phytochemistry* 50, no. 7 (1999): 1205–1208.

36. M. M. Abdelmageed, R. N. El-Naga, E. El-Demerdash, and M. M. Elmazar, "Indole-3-carbinol Enhances Sorafenib Cytotoxicity in Hepatocellular Carcinoma Cells," *Scientific Reports* 6 (2016): 32733, https://doi.org/10.1038/srep32733.

37. B. B. Aggarwal and H. Ichikawa, "Molecular Targets and Anticancer Potential of Indole-3-Carbinol," *Cell Cycle* 4, no. 9 (2005): 1201–1215, https://doi.org/10.4161/cc.4.9.1993.

38. N. Fujioka, V. Fritz, P. Upadhyaya, F. Kassie, and S. S. Hecht, "Research on Cruciferous Vegetables, indole-3-carbinol, and Cancer Prevention: A Tribute to Lee W. Wattenberg," *Molecular Nutrition & Food Research* 60, no. 6 (2016): 1228–1238, https://doi.org/10.1002/mnfr.201500889.

39. E. Katz, S. Nisani, and D. A. Chamovitz, "Indole-3-carbinol: A Plant Hormone Combatting Cancer," *F1000Research* 7 (2018): 689, https://doi.org/10.12688/f1000research.14127.1.

40. Y. A. Fouad and C. Aanei, "Revisiting the Hallmarks of Cancer," *American Journal of Cancer Research* 7, no. 5 (2017): 1016–1036.

41. M. A. Allen, Z. Andrysik, V. L. Dengler, et al., "Global Analysis of p53-regulated Transcription," *eLife* 3 (2014): e02200, https://doi.org/10.7554/eLife.02200.

42. E. R. Kastenhuber, G. Lalazar, S. L. Houlihan, et al., "DNAJB1–PRKACAfusion Kinase Interacts With β-catenin and the Liver Regenerative Response to Drive Fibrolamellar Hepatocellular Carcinoma," *Proceedings of the National Academy of Sciences* 114, no. 50 (2017): 13076–13084, https://doi.org/10.1073/pnas.1716483114.

43. A. Halina, P. Artur, M. K. Barbara, S. Joanna, and D. Anna, "TP53, Cyclin D2, C-Myc, p21 and p27 Alterations in B-CLL Progression," *Folia Histochemica et Cytobiologica* 48, no. 4 (2010): 534–541, https://doi.org/10.2478/v10042-010-0048-5.

44. L. C. Trotman and P. P. Pandolfi, "PTEN and p53: Who Will Get the Upper Hand?," *Cancer Cell* 3, no. 2 (2003): 97–99, https://doi.org/10.1016/s1535-6108(03)00022-9.

45. G. P. Dotto, "Crosstalk of Notch With p53 and p63 in Cancer Growth Control," *Nature Reviews Cancer* 9, no. 8 (2009): 587–595, https://doi.org/10.1038/nrc2675.

46. F. Liang, C. Ren, J. Wang, et al., "The Crosstalk Between STAT3 and p53/RAS Signaling Controls Cancer Cell Metastasis and Cisplatin

Resistance via the Slug/MAPK/PI3K/AKT-mediated Regulation of EMT and Autophagy," *Oncogenesis* 8, no. 10 (2019): 59, https://doi.org/10.1038/s41389-019-0165-8.

47. T. Ozaki, S. Ikeda, A. Kawai, H. Inoue, and T. Oda, "Alterations of Retinoblastoma Susceptible Gene Accompanied by C-Myc Amplification in Human Bone and Soft Tissue Tumors," *Cellular and Molecular biology (Noisy-le-Grand, France)* 39, no. 2 (1993): 235–242.

48. A. Montfort, C. Colacios, T. Levade, N. Andrieu-Abadie, N. Meyer, and B. Ségui, "The TNF Paradox in Cancer," *Frontiers in immunology* 10 (2019): 1818, https://doi.org/10.3389/fimmu.2019.01818.

49. X. Wang and Y. Lin, "Tumor Necrosis Factor and Cancer: Buddies or Foes?," *Acta Pharmacologica Sinica* 29, no. 11 (2008): 1275–1288, https://doi.org/10.1111/j.1745-7254.2008.00889.x.

50. A. S. H. da Silva Guerra, D. J. do Nascimento Malta, L. P. Morais Laranjeira, et al., "Anti-Inflammatory and Antinociceptive Activities of Indole-Imidazolidine Derivatives," *International Immunopharmacology* 11, no. 11 (2011): 1816–1822, https://doi.org/10.1016/j.intimp.2011.07.010.

51. C. Wang and R. J. Youle, "The Role of Mitochondria in Apoptosis," *Annual Review of Genetics* 43 (2009): 95–118, https://doi.org/10.1146/annurev-genet-102108-134850.

52. S. Xiong, T. Mu, G. Wang, and X. Jiang, "Mitochondria-Mediated Apoptosis in Mammals," *Protein & Cell* 5, no. 10 (2014): 737–749, https://doi.org/10.1007/s13238-014-0089-1.

53. M. A. Benavides, K. L. Hagen, W. Fang, et al., "Suppression by L-Methionine of Cell Cycle Progression in Lncap and MCF-7 Cells but Not Benign Cells," *Anticancer Research* 30, no. 6 (2010): 1881–1885.

54. Y. Liu and W. F. Bodmer, "Analysis of P53 Mutations and Their Expression in 56 Colorectal Cancer Cell Lines," *Proceedings of the National Academy of Sciences* 103, no. 4 (2006): 976–981.

55. M.-R. B. S. Crombag, S. L. W. Koolen, S. Wijngaard, et al., "Does Older Age Lead to Higher Risk for Neutropenia in Patients Treated With Paclitaxel?," *Pharmaceutical Research* 36, no. 12 (2019): 163.

56. H. Shigematsu, T. Hirata, M. Nishina, D. Yasui, and S. Ozaki, "Cryotherapy for the Prevention of Weekly Paclitaxel-Induced Peripheral Adverse Events in Breast Cancer Patients," *Supportive Care in Cancer* 28, no. 10 (2020): 5005–5011.

57. X. Zhang, J. Huang, C. Yu, et al., "Quercetin Enhanced Paclitaxel Therapeutic Effects Towards PC-3 Prostate Cancer Through ER Stress Induction and ROS Production," *OncoTargets and Therapy* 13 (2020): 513–523.

58. S. Vignarajan, C. Xie, M. Yao, et al., "Loss of PTEN Stabilizes the Lipid Modifying Enzyme Cytosolic Phospholipase A2α via AKT in Prostate Cancer Cells," *Oncotarget* 5, no. 15 (2014): 6289–6299.

59. T. Ogawa, K. Shiga, S. Hashimoto, T. Kobayashi, A. Horii, and T. Furukawa, "APAF-1-ALT, a Novel Alternative Splicing Form of APAF-1, Potentially Causes Impeded Ability of Undergoing DNA Damage-Induced Apoptosis in the LNCaP Human Prostate Cancer Cell Line," *Biochemical and Biophysical Research Communications* 306, no. 2 (2003): 537–543.

60. A. Calderon-Aparicio, A. Cornejo, A. Orue, and M. Rieber, "Anticancer Response to Disulfiram May Be Enhanced by Co-Treatment With MEK Inhibitor or Oxaliplatin: Modulation by Tetrathiomolybdate, KRAS/BRAF Mutations and c-MYC/p53 Status," *Ecancermedicalscience* 13 (2019): 890.

61. S. Alzahrani, H. Al Doghaither, Al-A. Pushparaj, and P. Al-ghafari, "5-Fluorouracil and Capecitabine Therapies for the Treatment of Colorectal Cancer (Review)," *Oncology Reports* 50, no. 4 (2023): 175.

62. Y. Yasuda, M. Saito, T. Yamamura, T. Yaguchi, and T. Nishizaki, "Extracellular Adenosine Induces Apoptosis in Caco-2 Human Colonic Cancer Cells by Activating caspase-9/−3 via A2A Adenosine Receptors," *Journal of Gastroenterology* 44, no. 1 (2009): 56–65.

63. C. T. Brew, I. Aronchik, J. C. Hsu, et al., "Indole-3-carbinol Activates the ATM Signaling Pathway Independent of DNA Damage to Stabilize p53 and Induce G1 Arrest of Human Mammary Epithelial Cells," *International Journal of Cancer* 118, no. 4 (2006): 857–868.

64. H. S. Choi, M. C. Cho, H. G. Lee, and D. Y. Yoon, "Indole-3-carbinol Induces Apoptosis Through p53 and Activation of caspase-8 Pathway in Lung Cancer A549 Cells," *Food and Chemical Toxicology* 48, no. 3 (2010): 883–890.

65. I. Aronchik, A. Kundu, J. G. Quirit, and G. L. Firestone, "The Antiproliferative Response of indole-3-carbinol in Human Melanoma Cells Is Triggered by an Interaction With NEDD4-1 and Disruption of Wild-Type PTEN Degradation," *Molecular Cancer Research* 12, no. 11 (2014): 1621–1634.

66. O. D. Reyes-Hernández, G. Figueroa-González, L. I. Quintas-Granados, et al., "3,3′-Diindolylmethane and indole-3-carbinol: Potential Therapeutic Molecules for Cancer Chemoprevention and Treatment via Regulating Cellular Signaling Pathways," *Cancer Cell International* 23, no. 1 (2023): 180.

67. C. Hong, H. A. Kim, G. L. Firestone, and L. F. Bjeldanes, "3,3′-Diindolylmethane (DIM) Induces a G1 Cell Cycle Arrest in Human Breast Cancer Cells That Is Accompanied by Sp1-mediated Activation of p21WAF1/CIP1 Expression," *Carcinogenesis* 23, no. 8 (2002): 1297–1305.

68. S. Harakeh, S. H. Saber, R. Al-Raddadi, et al., "Novel Curcumin Nanoformulation Induces Apoptosis and Reduces Migration and Angiogenesis in Liver Cancer Cells," *Artificial Cells, Nanomedicine, and Biotechnology* 51, no. 1 (2023): 361–370.

69. P. Manohong, N. Sornkaew, K. Meemon, et al., "Isolation of 3-(Hydroxyacetyl)indole and Indole-3-carboxylic Acid From Red Alga Halymenia Durvillei: Their Anti-Lung Cancer Cell and In Vivo Anti-Aging Activity," *Asian Journal of Chemistry* 33 (2021): 775–780.

70. Y. Q. Wang, C. Chen, Z. Chen, et al., "Indole-3-carbinol Inhibits Cell Proliferation and Induces Apoptosis in Hep-2 Laryngeal Cancer Cells," *Oncology Reports* 30, no. 1 (2013): 227–233.

71. O. D. Reyes-Hernández, G. Figueroa-González, L. I. Quintas-Granados, et al., "3,3′-Diindolylmethane and indole-3-carbinol: Potential Therapeutic Molecules for Cancer Chemoprevention," *Cancer Cell International* 23, no. 1 (2023): 180.

72. A. S. Baez-Gonzalez, J. A. Carrazco-Carrillo, G. Figueroa-Gonzalez, L. I. Quintas-Granados, T. Padilla-Benavides, and O. D. Reyes-Hernandez, "Functional Effect of indole-3-carbinol in Viability and Invasive Properties of Cancer Cells," *Biochemistry and Biophysics Reports* 35 (2023): 101492.

73. A.-M. Meredith and C. R. Dass, "Increasing Role of the Cancer Chemotherapeutic Doxorubicin in Cellular Metabolism," *Journal of Pharmacy and Pharmacology* 68, no. 6 (2016): 729–741.

74. F. Tokali, H. Senol, S. Atesoglu, and F. Akbas, "Quinazolin-4(3H)-one-morpholine Hybrids as Anti-Lung-Cancer Agents," *Chemical Biology & Drug Design* 104 (2024): e14599.

75. F. S. Tokalı, H. Şenol, Ş. Ateşoğlu, P. Tokalı, and F. Akbaş, "Polymethoxy Fenamate Isosteres as Novel Anti-Prostate Cancer Agents," *Journal of Molecular Structure* 1319 (2025): 139519.

76. M. Moussaoui, S. Baammi, H. Soufi, et al., "Design and Optimization of Quinazoline Derivatives as Potent EGFR Inhibitors for Lung Cancer Treatment: A Comprehensive QSAR, ADMET, and Molecular Modeling Investigation," *ACS Omega* 9, no. 46 (2024): 45842–45857.

77. S. Zareei, M. Mohammadi-Khanaposhtani, M. Adib, M. Mahdavi, and P. Taslimi, "Sulfonamide-Phosphonate Hybrids as Carbonic Anhydrase Inhibitors," *Journal of Molecular Structure* 1271 (2023): 134114.

78. S. Saikia and M. Bordoloi, "Molecular Docking: Challenges, Advances and Its Use in Drug Discovery Perspective," *Current Drug Targets* 20, no. 5 (2019): 501–521.

79. F. S. Tokalı, H. Şenol, Ş. Ateşoğlu, and F. Akbaş, "A Series of quinazolin-4(3H)-one-morpholine Hybrids as Anti-Lung-Cancer

Agents: Synthesis, Molecular Docking, Molecular Dynamics,ADME prediction and Biological Activity Studies," *Chemical Biology & Drug Design* 104, no. 1 (2024): e14599.

80. Z. Arslan, E. Okuroğlu, H. Şenol, and Z. Türkmen, "1-Benzhydrylpiperazine: Isolation, Structure Determination and In Silico Studies," *Journal of Food Composition and Analysis* 135 (2024): 106682.

81. M. Karplus and J. A. McCammon, "Molecular Dynamics Simulations of Biomolecules," *Nature Structural Biology* 9, no. 9 (2002): 646–652.

82. A. Şen, B. Ayar, A. Yilmaz, Ö. Ö. Acar, G. Ç. Turgut, and G. Topçu, "Natural Diterpenoid Alysine A Isolated Fromteucrium Alyssifoliumexertsantidiabetic Effect via Enhanced Glucose Uptake and Suppressed Glucose Absorption," *Turkish Journal of Chemistry* 43 (2019): 1350–1364.

83. S.-J. Lee, O. R. Hedstrom, K. Fischer, et al., "Immunohistochemical Localization and Differential Expression of Cytochrome P450 3A27 in the Gastrointestinal Tract of Rainbow Trout," *Toxicology and Applied Pharmacology* 177, no. 2 (2001): 94–102.

84. A. Sen and E. Arinc, "Purification and Characterization of Cytochrome P450 Reductase From Liver Microsomes of Feral Leaping Mullet (Liza Saliens)," *Journal of Biochemical and Molecular Toxicology* 12, no. 2 (1998): 103–113.

85. U. K. Laemmli, "Cleavage of Structural Proteins During the Assembly of the Head of Bacteriophage T4," *Nature* 227 (1970): 680–685.

86. V. Lezcano, C. Gentili, and A. R. de Boland, "Role of PTHrP in Human Intestinal Caco-2 Cell Response to Oxidative Stress," *Biochimica et Biophysica Acta (BBA)-Molecular Cell Research* 1833, no. 12 (2013): 2834–2843.

87. M. Sulak, G. C. Turgut, and A. Sen, "Cerium Oxide Nanoparticles Biosynthesized Using Walnut Shell: Anticancer Effect," *Chemistry & Biodiversity* 19, no. 8 (2022): e202200131.

88. G. Ç. Turgut, D. Doyduk, Y. Yıldırır, et al., "Computer Design, Synthesis, and Bioactivity Analyses of Drugs Like Fingolimod Used in the Treatment of Multiple Sclerosis," *Bioorganic & Medicinal Chemistry* 25, no. 2 (2017): 483–495.

89. H. Şenol, A. G. Ağgül, and S. Atasoy, "Synthesis, Characterization, Molecular Docking Andin Vitrobiological Studies of Thiazolidin-4-one Derivatives as Anti-Breast-Cancer Agents," *ChemistrySelect* 8, no. 20 (2023): e202300481.

90. Z. Yang, W. Wang, Y. Qi, et al., "New Catechin Derivatives as SARS-CoV-2 Mpro Inhibitors," *Computers in Biology and Medicine* 151 (2022): 106288.

91. H. Nada, K. Lee, L. Gotina, A. N. Pae, and A. Elkamhawy, "Identification of Novel DDR1 Inhibitors Using E-Pharmacophore Modeling," *Computers in Biology and Medicine* 142 (2022): 105217.

92. L. Shi, Z. Wen, Y. Song, J. Wang, and D. Yu, "Computational Investigation of SARS-CoV-2 nsp16 Inhibitors," *J Mol Graph* 117 (2022): 108306.

93. B. Zengin Kurt, D. Öztürk Civelek, E. B. Çakmak, et al., "Synthesis of Sorafenib−Ruthenium Complexes, Investigation of Biological Activities and Applications in Drug Delivery Systems as an Anticancer Agent," *Journal of Medicinal Chemistry* 67, no. 6 (2024): 4463–4482.

94. F. S. Tokalı, P. Taslimi, M. Sadeghi, and H. Şenol, "Synthesis and Evaluation of Quinazolin-4(3H)-one Derivatives as Multitarget Metabolic Enzyme Inhibitors: A Biochemistry-Oriented Drug Design," *ChemistrySelect* 8, no. 25 (2023): e202301158.

95. H. Şenol, M. Ghaffari-Moghaddam, G. Ö. Alim Toraman, and U. Güller, "Novel Chalcone-Ursolic Acid Derivatives as AChE Inhibitors," *Journal of Molecular Structure* 1295 (2024): 136804.

96. I. Mamedov, H. Senol, F. Naghiyev, V. Khrustalev, N. Sadeghian, and P. Taslimi, "New Tetrahydro-Isoquinoline Derivatives as Cholinesterase and α-glycosidase Inhibitors," *Journal of Molecular Liquids* 404 (2024): 125006.